UNIVERSITÀ DEGLI STUDI DI PADOVA

DIPARTIMENTO DI INGEGNERIA DELL'INFORMAZIONE

UNIVERSITY OF PADUA

Department of Information Engineering

Master degree in Bioengineering

Implementation of a calibration protocol for a BMI-driven robotic exoskeleton

Supervisor

Prof. Luca Tonin

Candidate

Valentino Marchesan

Co-Supervisor

Dr. Stefano Tortora

December 12, 2022

Academic Year 2021-2022

Università degli Studi di Padova

Dipartimento di Ingegneria dell'Informazione

Implementation of a calibration protocol for a BMI-driven robotic exoskeleton

Valentino Marchesan

Master Degree in:

Bioengineering

Supervisor:

Prof. Luca Tonin

Co-Supervisor:

Dr. Stefano Tortora

Date:

December 12, 2022

Abstract

Brain-machine interfaces (BMIs), based on electroencephalography (EEG), have been proved to play an important role in motor rehabilitation. BMIs can classify EEG signals and translate the brain activities into useful commands for external devices. The aim of this work is the creation and implementation of a calibration protocol for a BMI to control a lower-limb exoskeleton. In contrast with the literature, the innovative aspect of the proposed method is the achievement of a robotic-aided calibration protocol in which the EEG data are collected while the user is inside the exoskeleton. The idea is to minimize the difference in brain activity between the calibration phase and the effective usage of the system. In particular, a paradigm based on the self-paced attempt of stepping movements have been implemented and the experiment involved the participation of seven healthy subjects. The EEG signals collected were used to test the performances of three different classifiers (Linear Discriminant Analysis (LDA), Logistic Regression (LR), supervised Gaussian Mixture Model (sGMM)) and two features selection approaches (Fisher score (FS), Common Spatial Patterns (CSP)). Finally, an exponential integrator was used to better recognize the movement intention and were identified the best integrator parameters that maximize the true positive-false positive ratio on average on the considered population. I found that 1 s is a good time for the detection of a pre-movement state and the LDA

classifier works better than the others with a mean sample-by-sample accuracy of $59.2506\% \pm 3.7142$ and a mean cross entropy loss of 0.6669 ± 0.031. Then I found a mean true positive rate of $76.32\% \pm 10.05$ and a mean false positive rate of $31.46\% \pm 24.20$. I believe that neuro-controlled exoskeleton will be the key solution to improve the quality of life of people with walking impairments.

Copyright ©2022, by Valentino Marchesan
all rights reserved.

Contents

List of Figures

List of Tables

List of Acronyms

ACC Anterior Cingulate Cortex.

AI Artificial Intelligence.

AUC Area Under the Curve.

BCI Brain-Computer Interface.

BMI Brain-Machine Interface.

BWS Body Weight Support.

CSP Common Spatial Pattern.

DoF Degree of Freedom.

EEG Electroencephalography or Electroencephalogram.

EMG Electromyographic.

EOG Electrooculogram.

EP Evoked Potentials.

ERD Event-related Desynchronisation.

ERP Event-related Potentials.

ERS Event-related Synchronisation.

fMRI Functional Magnetic Resonance Imaging.

FN False Negative.

fNIRS Functional Near-Infrared Spectroscopy.

FP False Positive.

FPR False Positive Rate.

FTC Fundamental Theorem of Calculus.

FTT Fast Fourier Trasform.

GMM Gaussian Mixture Model.

GUI Graphical User Interface.

iEEG Intracranical Electroencephalography.

LDA Linar Discriminant Analysis.

LR Logistic Regression.

MA Movement Attempt.

ME Motor Execution.

MEG Magnetoencephalography.

MI Motor Imagery.

MLE Maximum Likelihood Estimation.

NF Neurofeedback.

PET Positron Emission Tomography.

PSD Power Spectral Density.

ROS Robot Operating System.

SD Standard Deviation.

SGMM supervised Gaussian Mixture Model.

SMR Sensorymotor Rhythm.

SSVEP Steady State Visual Evoked Potentials.

TN True Negative.

TP True Positive.

TPR True Positive Rate.

1 | Introduction

According to the Oxford English Dictionary, the term "rehabilitation" has many definitions, and that relating to the semantic area of medical health considers rehabilitation as the "restoration to some degree of normal life by appropriate training" [1]. Medical rehabilitation is the process targeted to promote and facilitate the recovery from physical damage, psychological and mental disorders, and clinical disease [2]. The World Health Organization considers disabilities as an umbrella term that covers impairments, activity limitations, and participation restrictions. An impairment is a problem in body function or structure, an activity limitation is a difficulty encountered by an individual in executing a task or action, while a participation restriction is a problem experienced by an individual when involved in everyday-life situations. So the physical problem becomes also a social problem.

Lower limb disability can have various origins, either medical (e.g., stroke [3], multiple sclerosis [4] or Parkinson's disease [5]) or traumatic (e.g., spinal cord injury [6]). In these conditions, either leg muscles become inefficient for walking or the brain motor signals do not even properly reach the spinal motoneurons commanding the leg muscles. The consequences are similar: the disabled person cannot properly stand up or walk autonomously anymore. One of the aim of the rehabilitation engineering is to restore a comfortable life to these people with disabilities. This can be done through the development

of technological tools to empower the lower limbs of disabled people with walking disability. This will drastically change their day-to-day life, as they will perform most usual daily activities more independently, both at home and outside. This is very important because brings to their own inclusion in society [7].

In recent years, with the current advancements in robotics and Artificial Intelligence (AI), robots have the potential to support the field of healthcare. Robotic systems are often introduced in the care of the elderly, children, and persons with disabilities, in hospitals, in rehabilitation and walking assistance, and other healthcare situations [8]. In the context of assisted rehabilitation through the use of robotic devices, the exoskeletons can be introduce, because it is used to restore the natural gait to people with lower limb impairments [9]. The lower limb rehabilitation exoskeleton is connected with the human body in a wearable way and can control the movement of all joints in the training process. According to their application, these robots are divided into two types, namely for treadmill-based and overground applications [10]. Patients can receive gait training from treadmill-based exoskeleton robots on a treadmill. In these robots, in addition to the exoskeleton that is used to provide assistance to leg movement, a body weight support (BWS) system is required to reduce gravitational forces acting on the legs, ensuring safety, and maintaining balance; the most famous exoskeleton on a treadmill is the Lokomat (Figure 1.1). Overground exoskeleton robots help patients in regaining overground gait; in this thesis I will focus on this type of exoskeletons (see Chapter 3.1.3).

Very important was the discovery of training-induced plastic changes in the functional topography of the primary motor cortex [11]. This has provided new opportunities for neurorehabilitation: the strategy of intensive, regular

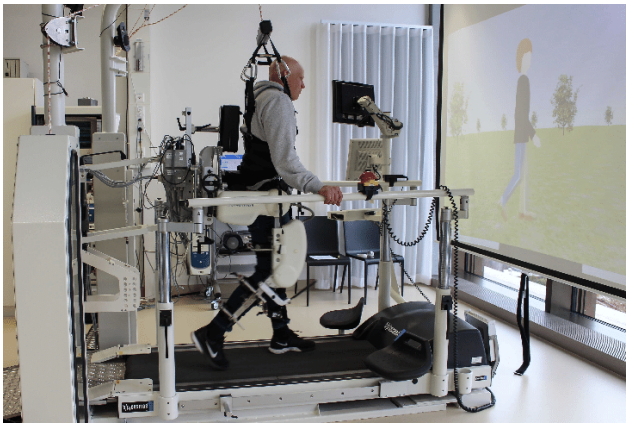

Lokomat

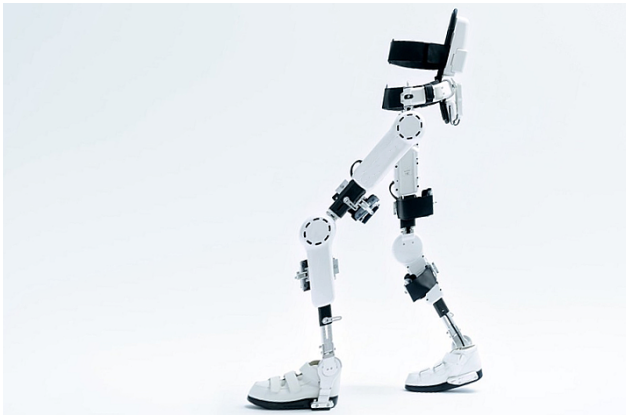

Cyberdine's HAL

Figure 1.1: Treadmill-based and overground exoskeletons

and motivated movement training has been developed. Exoskeletons appears to be ideal technical devices for this strategy implementation.

The traditional control mode for exoskeleton robots is based on physical sensor signals, such as accelerometers, IMUs, and potentiometers. In recent years, biological signals such as the electroencephalography (EEG) signal through the brain-machine interface (BMI) have become a new method for human-machine interaction in rehabilitation robots [12]. This leads to the introduction of a new multi-disciplinary research field known as neuro-

robotics. Neurorobotics refers to the branch of science combining neuroscience, robotics, and artificial intelligence. It hence refers to all robots developed for interacting with or for emulating the nervous system of humans or other animals. A neurorobot can be developed for clinical purposes, for example neurorehabilitation or neurosurgery [13]. The main features of the neurorobots belonging to the walking assistance category are the ability to allow the patient to physically (or virtually) navigate the environment, either indoor or outdoor, and the capability to partially (lower-limb exoskeleton, leg prostheses) or totally (powered wheelchair) support their weight to alleviate fatigue due to possible disorders.

The closed-loop control of rehabilitative technologies by neural commands has shown a great potential to improve motor recovery in patients suffering from paralysis [14]. BMIs can be used as a natural control method for such technologies. BMI provides a continuous association between the brain activity and peripheral stimulation, with the potential to induce plastic changes in the nervous system. Paraplegic patients constitute a potential target population to be rehabilitated with brain-controlled robotic systems, as they may improve their gait function after the reinforcement of their spared intact neural pathways [14].

Following this line, in this thesis I firstly created a protocol for the EEG signals acquisition and adjust the exoskeleton software to allow a walk of the robot as is defined in the protocol. Then I studied the EEG of people that walked with exoskeleton. Finally, I define a machine learning-based classifier of the EEG signal's features which target is to identify the onset of a movement of the person. This because the next step of the project will be to create an online closed-loop control of the exoskeleton that allows a person to trigger the exoskeleton assistance through the identification of walking

intention from brain activity.

2 | State of the art

2.1 Brain Machine Interface

Physical disability caused by neurologic disease is the reason while neurorehabilitation born. The conditions that are most frequently encountered on a neurorehabilitation service are stroke, traumatic head injury, spinal cord injury, multiple sclerosis, Parkinson's disease, and devastating peripheral neuropathies. The aim of neurorehabilitation is improve patients' ability to perform daily activities and self-care and to achieve functional independence [15]. One method to restore the ability of the patient is neurofeedback. Neurofeedback (NF) is a non-invasive close-loop technique that take information from EEG activity that is recorder by a low number of electrodes; after the acquisition there is a little computation, and this activate some output which are then captured from the patient. NF targets the brain and cognitive functions through the use of electroencephalography (EEG), hence neurofeedback is sometimes referred to as EEG biofeedback. In classical NF, EEG and brainwave activity is provided as a visual or auditory cue to the user. Using these cues the user can consciously adapt their brainwave activity to reach targeted training thresholds. NF relies on operant conditioning to stimulate the neuroplastic abilities of the brain. Physiologically stimulating specific band frequencies over damaged areas stimulates cortical metabolism.

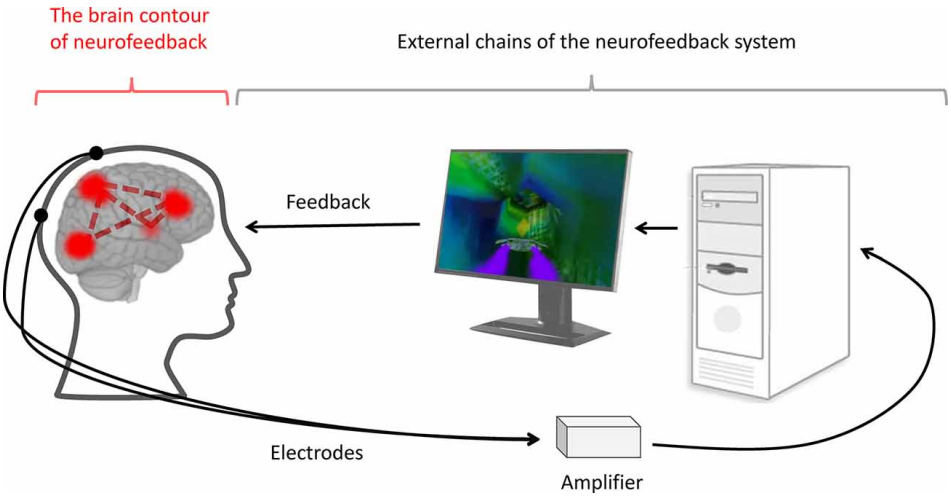

Figure 2.1: Neurofeedback scheme

NF is also used to counter excessive slow wave activity (i.e. theta waves and sometimes alpha waves) that typically follow stroke [16]. In Figure 2.1 is shown the functioning of neurofeedback [17].

Another neurorehabilitation method is brain-machine Interface (BMI) also called brain-computer Interface (BCI). The term BMI refers to a system capable of measuring the activity of the brain and translating it into instructions for various types of peripheral devices (wheelchairs [18], prostheses [19] and orthoses [20]); in fact brain-machine interfaces give their users communication and control channels that do not depend on the brain's normal output channels of peripheral nerves and muscles [21]. For this the BMI provides an alternative interaction channel for people suffering from severe motor disabilities by circumventing the normal-usually damaged neural pathways [22, 23]. BMIs are based on neurofeedback. For this reason, it could take in consideration that neurofeedback is a container of BMIs technology. Both could induce plasticity and enable control of brain activity in a closed loop. However, there are many differences: neurofeedback is just a mirror on our brain activity, there is any multivariate association. Neurofeedback is only one way

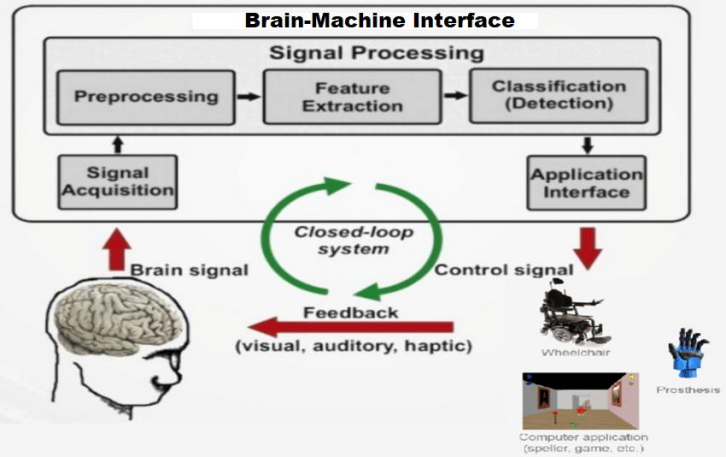

Figure 2.2: BMI close-loop scheme

directional, in fact, is only the subject that know how to modulate the signal, while, in BMI are also implemented some machine learning algorithms in which the BMIs learn from the patients' neural data. This concept of learn how to use the BMI and the learning process of BMI about the patient's behaviour is called mutual learning [24]. Moreover, another difference between BMI and neurofeedback is the number of electrodes used, which is usally much higher in the BMI context.

As neurofeedback, also BMI is based on a closed-loop architecture [25] (Figure 2.2) where user and machine interact with each other to achieve optimal control of the external device, but in BMI the user's intentions are translated not into virtual movements of an abstract element on a screen, but rather into tangible actions of a device. Two concepts therefore become essential in the design of the BMI closed-loop: a fast response by the robot to the user's intention and a bidirectional interaction between the robot and BMI.

As it can seen in Figure 2.2, the closed-loop architecture is composed by three main blocks:

- **Signal acquisition**: deal with the acquisition of the EEG signal that

can be done in an invasive or non-invasive way;

- **Signal Processing**: this block can be divided in three sub-blocks:
  - Preprocessing: which role is filtering, downsampling, remove the artifact, interpolating the channels and re-referencing the EEG raw signals;
  - Features Extraction: which aim is to determine and select the most discriminant features;
  - Classification: which classify the extracted features.

- **Feedback**: generate actions of the external device and provide the results of the actions back to the user.

Signal acquisition

In BMI systems there are two possible types of signal acquisition: invasive or non invasive. Invasive BMIs can directly access the spiking activity of single neurons or local field potentials by means of microelectrodes implanted at the cortical or subcortical level (iEEG) [26]. Less invasive acquisition techniques rely on electrocorticogram signals read by electrodes placed on the surface of the cortex. Although invasive recordings allow high spatial and temporal resolution, signal quality may be affected by the reaction of the cerebral tissue to the implant [27]. The non-invasive BMI are based on technologies that scan the brain without surgery and invasive techniques, such as as Functional magnetic resonance imaging (fMRI) or Functional near-infrared spectroscopy (fNIRS) or other technique like EEG and Magnetoencephalography (MEG). FMRI is a technology that could detect the major brain area which contains

the main concentration of blood oxygenated [28]. This technique has a high spatial resolution but a low temporal resolution. This last aspect is quite important to obtain rapid response from the technology. With this characteristic the technique cannot be used to implement BMI paradigms. FNIRS is similar to fMRI with the only difference to have as acquisition component a cap and not very big, large coil [29]. The concept is very similar to fMRI, in fact, also in this case, the technology could help to detect the main brain region which present the highest concentration of blood oxygenated. So, this technology has high spatial resolution but, for the same reason of fMRI slowness, it has low temporal resolution. MEG is a technique that could help to achieve the detection of a very low amplitude magnetic fields [30]. This technology has high spatial and temporal resolution but low usability due to the use of superconducting quantum interference devices (SQUIDs) to detect the neuromagnetic field. A positron emission tomography (PET) scan is an imaging test that can help to reveal the metabolic or biochemical function of tissues and organs [31]. The PET scan uses a radioactive drug (tracer) to show both normal and abnormal metabolic activity. A PET scan can often detect the abnormal metabolism of the tracer in diseases before the disease shows up on other imaging tests, such as fMRI. A PET scan is an effective way to help to identify a variety of conditions, including cancer, heart disease and brain disorders. In this case it isn't use due to the high time resolution needed. Electroencephalogram (EEG) measures the electrical activity of a population of neurons by the usage of cap of electrodes. It has low spatial resolution due to the physical dimension of electrodes. Nowadays the maximum number of electrodes is 256 in the most advance EEG system. The ones used in clinical practice consist normally of 64 electrodes to speed up the wearing process. So the reasons why the EEG is the most used acquisition

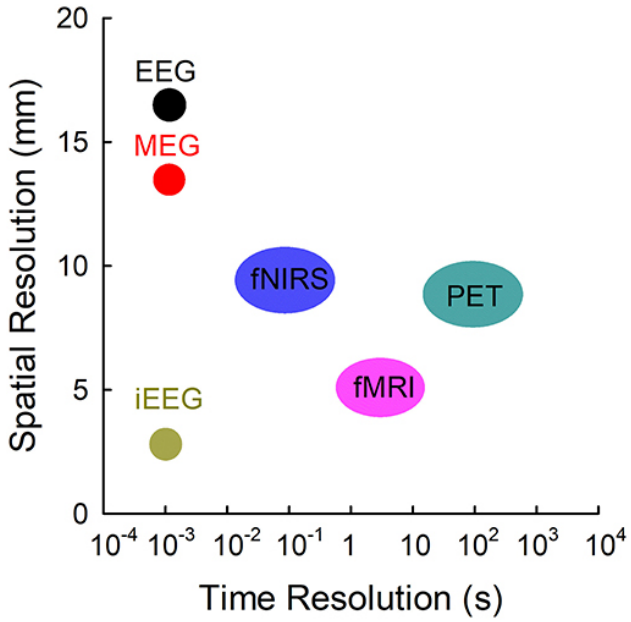

Figure 2.3: Spatial and temporal resolution of different type of acquisition techniques

technique in BMI is that it has high temporal resolution, high usability, and low access cost. The scheme in Figure 2.3 represents the resolution of the different techniques that could be used to record the brain activity [32].

2.1.1 Electroencephalography (EEG)

For the reason already explained (low cost, high usability, high temporal resolution) my BMI system will use the EEG as signal acquisition technique. An EEG sensor is a non-invasive electronic device that can measure electrical signals of the brain. EEG sensors typically measure the varying electrical signals created by the activity of large groups of neurons (cortical pyramidal cells) near the surface of the brain, that have to fire in synchrony to generate a signal detectable by the electrodes. They work by measuring the small fluctuations in electrical current between the skin and the sensor electrode [33]. In the EEG measurements, the cerebral cortex is the most relevant

structure, and it is responsible for high order cognitive tasks (problem solving, language comprehension, movement and processing of complex visual information). Due to its surface position, the electrical activity of the cerebral cortex has the greatest influence on EEG recordings. EEG measures the difference in voltage over the scalp in microvolt (µV).
EEG signals have two mainly characteristics: amplitude and frequency. The Brain waves have commonly a sinusoidal shape. Usually, they are measured from peak to peak and normally range from 0.5 to 100 µV in amplitude. From a spectral point of view, the EEG signal occupies a frequency range between 0.1 Hz and 100 Hz. The brain waves can be categorized into five basic groups (Figure 2.4) in different frequency range [34]:

- Delta (0.5-4 Hz): it tends to be the highest in amplitude and the slowest waves. It is normal as the dominant rhythm in infants up to one year

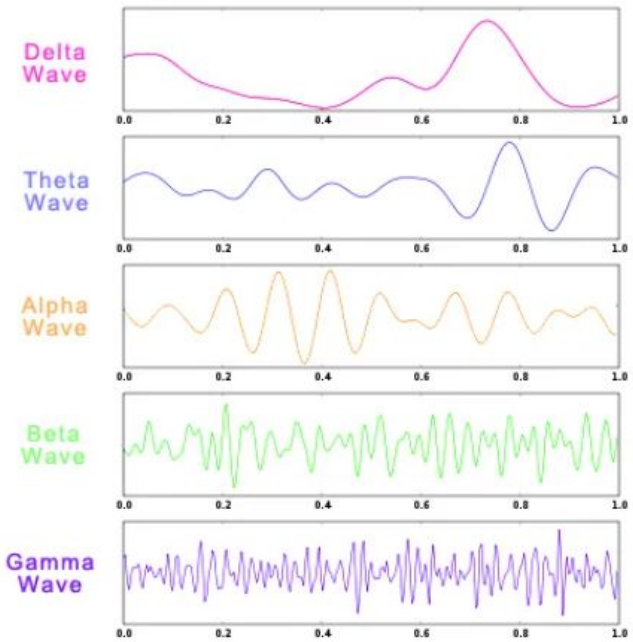

Figure 2.4: Brainwaves

and in stages 3 and 4 of sleep. It is usually most prominent frontally in adults and posteriorly in children;

- Theta (4-8 Hz): it is perfectly normal in children up to 13 years and in sleep but abnormal in awake adults. It can be recorder using temporal and frontal electrode;

- Alpha (8-13 Hz): it appears when closing the eyes and relaxing, and disappears when opening the eyes or alerting by any mechanism; it is the major rhythm seen in normal relaxed adults. It is usually best seen in the posterior regions of the head on each side, being higher in amplitude on the dominant side;

- Beta (13-30 Hz): it is the dominant rhythm in patients who are alert or anxious or have their eyes open. Beta rhythm is also associated with motor activity, and is modulated during both real movement and motor imagination. It is usually seen on both sides in symmetrical distribution and is most evident frontally. It is generally regarded as a normal rhythm.

- Gamma (>30 Hz): it occurs in relation to certain motor functions as during maximal muscle contraction and during high cognitive tasks. Gamma rhythm are less used in EEG based BCI systems because they are more susceptible to muscular or EEG artefacts.

It is important to notice that with the increment of frequency, the amplitude of the signal decreases following a $1/f$-like trend, as shown in Figure 2.5. So the Delta waves have the biggest amplitude in µV, while the Gamma waves the smallest.

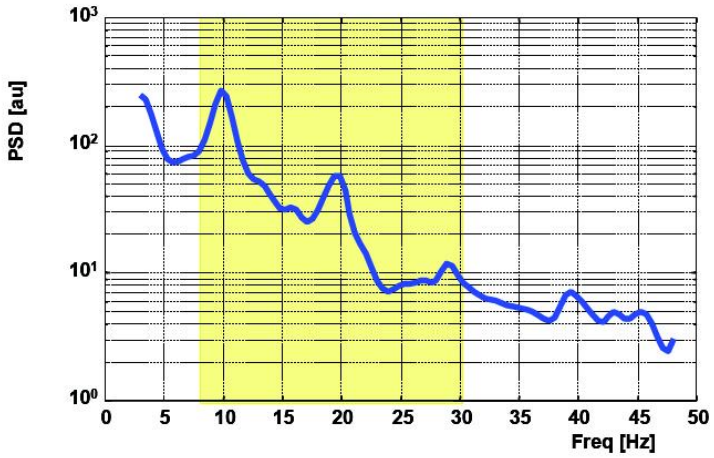

Figure 2.5: $\frac{1}{f}$ trend of the EEG spectrum

The main characteristic that could be retrieved from Figure 2.5 is that there is an alpha peak which is around 10 Hz, whose precise position in frequency is strongly subject-specific. The next structure after the alpha peak that could be detected is an another rebound which is usually call the beta peak and it is present according to the specific task. This rebound in beta synchronization is observed after the end of voluntary movements as well as after somatosensory stimulation and is believed to describe the return to baseline of sensorimotor networks [35]. It could be seen that in the gamma range the amplitude of the component is small and has a high risk to be overlapped with the muscular electrical activity from neck muscle, and thus they are rarely used in BMI applications.

2.1.2 BMI based on EEG modulation

The activity of the EEG can be influenced and modulated by different methods. There are mainly two ways that can be used to do that and that are involved in the BMI system: the *Event-related Potentials (ERP)* [36] and the *Spontaneus signals* [37]:

- Event-related potentials (ERP): they are potential difference fluctuations that are both time-locked and phase-locked to a discrete physical, mental, or physiological occurrence, referred to as the event. They are called also evoked phenomena;

- Spontaneus signals: they are time-locked phenomena but are not phase-locked, because they are endogenous of the patient. It is possible to refer to them as induced phenomena.

Event-related potentials

The Event-related potentials, also called evoked potentials (EP), are the measurement of brain responses to specific external event [38]. It is a sensitive and qualified neurophysiopathological investigation technique, which provides and objective measure of the functioning of specific sensory nerve pathways (visual, acoustic, sensory). EPs are usually described as a number of positive and negative peaks characterized by their polarity, shape, amplitude, latency and spatial distribution on the scalp. All these characteristics depend on the type of event. Each realization of an EP is named a sweep or trial. Mathematically they could be described as:

$$y(t) = v(t) + u(t)$$

where $v(t)$ component is the EP and the $u(t)$ is the noise which is contained into the EEG signal due to the other brain activities active during the elaboration. The signal is time-locked to the stimulus and most of the noise occurs randomly, allowing the noise to be averaged out with averaging of repeated responses :

$$\widehat{u}(t) = \frac{1}{N} \cdot \sum N \cdot y_i(t)$$

The most common EPs used in BMI are the following:

- ***Steady State Visual Evoked Potentials (SSVEP)*** [39]: it is a very simple technique. The key point is that if there are two stimuli (leds) that are blinking at a certain frequency, could be find an oscillatory pattern and frequency component in the occipital region depending on the frequency of the led that is paying attention to. The frequency of the component that is find in the occipital region is the same of the flickering frequency of the stimulus. In this case may have different kind of visual stimuli each connected to a different action and activity;

- ***P300***: the P300 could be triggered by an exogenous visual or audio stimulation [40]. P300 evoked potential is the manifestation of attention-involved activity (cognitive process). An example of technique to elicit a P300 is made up of a time presentation of square target which are interspersed by square non target. It is asked to the user to count all the target square and by doing so, the patient is paying attention to the sequence and each time the target stimulus is presented a P300 EP is elicited. A key point of the series presented is that the target stimulus needs to be presented randomly. This activity could also be done by the usage of sound stimulation. The P300 appears after 300 ms of latency from the onset;

- ***Error potentials***: when there is the detection of an erroneous stimulus (identifiable by only a cognitive process) an error potential is evoked [41]. This last type of EP is elicited in the anterior cingulate cortex (ACC) and comes out after 100-200 ms after the error recognition. By detecting this EP could be reacted to this information by modify the

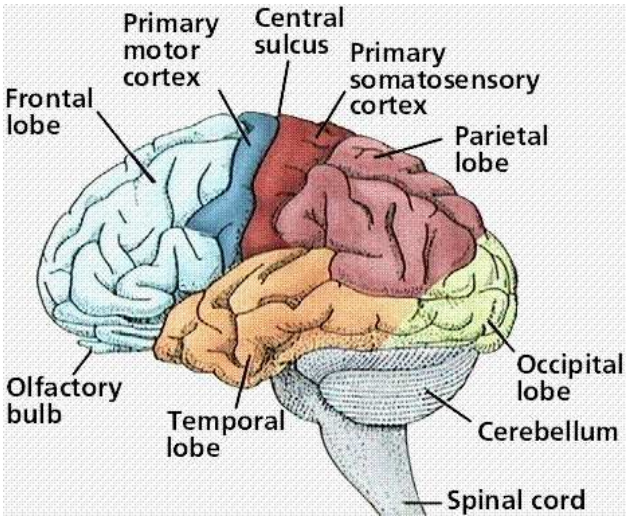

(a)

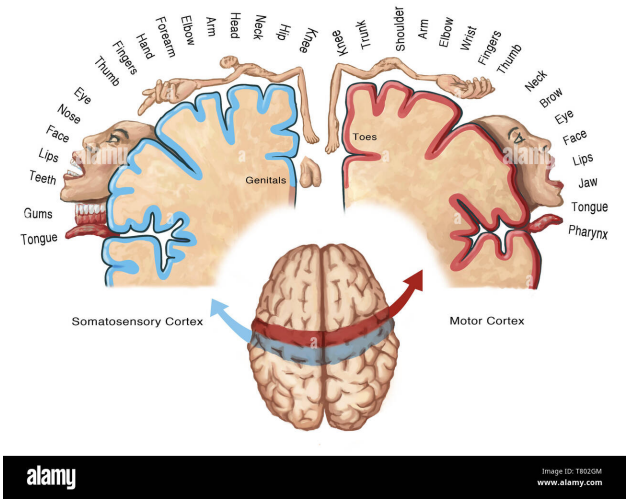

(b)

Figure 2.6: Cortical organization (a), Motor homunculus (b)

behaviour of the system in order to correct wrongly executed actions of the BMI system.

Spontaneus signals

Spontaneous signals are the brain modulation generated spontaneously/voluntarily by the subject without any external stimulation. Part of this family of signals are: sensorimotor rhythms (SMR), slow cortical potentials and cortical neuronal action potential; these signals are mostly related to motor activities and thus their are mostly visible over the sensorimotor cortex (Figure 2.6a). As shown in the Figure 2.6a there are different lobes in the cortex which are referred to specific brain activity. Every brain region is specific to detect a particular brain rhythm. The most important area for BMI technology is the sensorimotor cortex [42]. In this specific region could be find a specific organization which is called the homunculus-motorius where all the segments of our body are represented. In Figure 2.6b is reported the organization of the sensorimotor area.

Motor execution and motor imagery can be decoded from the sensorimotor rhythms [43], which forms the basis of neural control in SMR-based BMIs, where

- **Motor imagery (MI)**: is the the kinesthetics imagination of the movement, so it fell like that it is doing that movements but the activity is blocked and this block does not allow the real motor execution;
- **Motor execution (ME)**: is the real movement.

The main difference between these two sensorimotor signals are that motor execution and motor imagination do not activate the same brain regions [44, 45]. Studies have demonstrated that people can learn to modulate their sensorimotor signals to control physical or virtual devices [43, 46]. Another important fact is that SMR are readily detectable in healthy as well as disabled individuals with neuromuscular diseases or injuries [47], so it is possible

to use SMR-based BMI in the rehabilitation process. Task related modulation in sensorimotor rhythms is usually manifested as amplitude (or power) decrease in the alpha-beta band components before the movement execution, also known as event-related desynchronization (ERD) [43]. To describe more mathematically the rest and movement condition, Pfurtsheller introduced a formula to quantify the power of the cerebral event analysed when a specific condition occurs [48]. In particular this relation is able to distinguish two different cases:

- Event related synchronization (ERS): that reflects a cortical "idling state", they are produced by synchronous activation of the neuronal network and they are associated with activity increase (positive values). This condition arises when the patients is in a rest condition.

- Event related desynchronization (ERD): instead indicates oscillations in cortical activation and asynchronous activation of the neuronal network. They are associated with activity decrease of the underline neuronal population (negative values). The ERD especially manifests in α and β bands during movement.

The analytical expression introduced by Pfurtsheller is:

$$ERP_x = \frac{P_{x,active} - P_{x,rest}}{P_{x,rest}} \times 100 \tag{2.1}$$

where positive values represent ERS while negative values the ERD. Before and during the movement, could be had an ERD over the primary motor cortex while during the rest phase could found an ERS over the sensorimotor cortex. Planning and execution of movement has been found to lead to predictable decreases in the alpha and beta frequency bands [48]. Also, many studies have demonstrated that motor imagery and motor execution

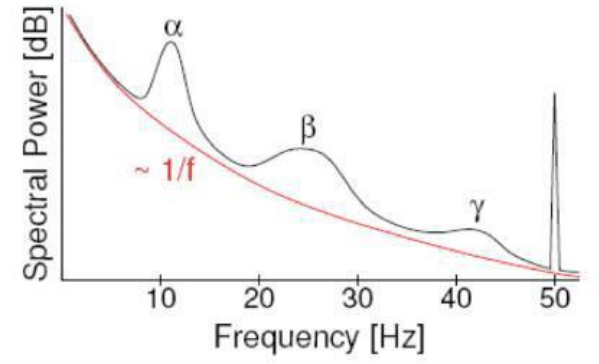

(a)

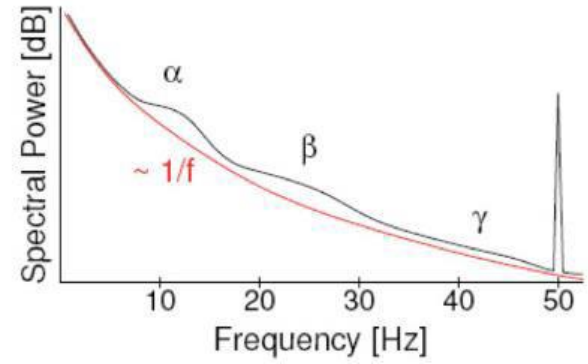

(b)

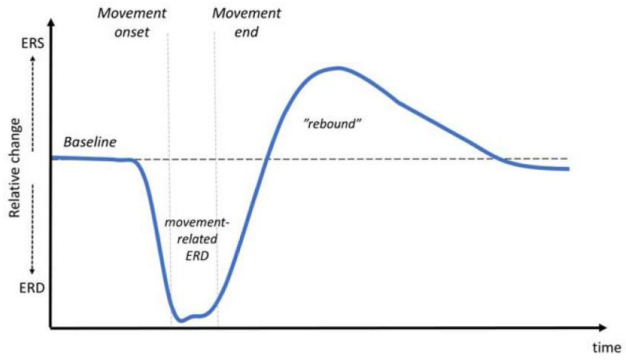

(c)

Figure 2.7: PSD during rest state (a), PSD during a MI/ME task (b), Beta-rebound (c)

can cause ERD (and often ERS) in primary sensorimotor areas [49]. To identify these brain rhytms could be seen that during motor imagination

or execution task, there is an attenuation of the activity of corresponding brain areas. This attenuation is the one that could be find during the spectral power analysis. For example, during the imagination hand movement the desynchronizations activated (ERD) lead to an attenuation of the main alpha peak. This is due to the desynchronization of the populations of neurons that take part to the subject mental tasks. During MI and ME task the spectral power density is characterised of a attenuation in alfa and beta band (Figure 2.7), while if we analysed the power spectral density compute during a cognitive task we will see a development of a peak in gamma band. The reason is due to the recruitment of different populations of neurons. In fact, it has been shown that during a MI or a ME task neurons or populations of these, works not in synchrony and this leads to an attenuation of the alfa and beta band, while during cognitive process due to the high specificity of the task the number of neurons recruited are just a few but these works in synchrony [48, 44, 49, 50]. One more thing that need to be highlighted, that was reported also at the end of 2.1.2 section and that is possible to see in Figure 2.7, is that when it is speaking of MI and ME is that after the ERD in the EEG could be detected, after 300-500ms, a beta rebound which represents the end of the movement and the activation of cognitive feedback, so a new synchronisation of neurons [51]. An important derivation of motor execution is the movement attempt (MA), in fact many of the robot-assisted motor rehabilitation therapies rely on the patient's attempt to move, based on residual movements. Usually rehabilitation based on this sensorymotor rhytm uses the combination of a EEG signal and an EMG signal to establish when the patient try to move himself. This SMR signal can be used for the rehabilitation of patient that have some residual movements and with the use of a neurorobots driven by a BMI the movement can be completed when

the BMI detect the moving intention of the patient.

2.2 Related works

Recent engineering and neuroscience applications have led to the development of BMI systems that improve the quality of life of people with motor disabilities [52]. In the same area, a significant number of studies have been conducted in identifying or classifying upper-limb movement intentions. On the contrary, a few works have been conducted concerning the identification of movement intention for lower limbs, in particular to control lower limb exoskeletons [53].

2.2.1 Motor imagery

In [54] the aim was distinguish motor imagery (MI) of flexion and extension of both legs from the EEG correlates, to control with a BMI a lower-limb gait training exoskeleton. The experimental protocol is composed by two sessions for each run: one offline session for training and one online session for the validation. Each session consists of five successive runs with a rest period in between. In each run, trials of extension and flexion were randomized and balanced and a total of 60 trials were performed (around 10min). During the experiment, the subject was seated in a customized gait training exoskeleton with a monitor in front of the robot. The visual cues were presented with a customized script and synchronized with the lower-level routines. Visual bars pointing upwards indicated leg extension MI and downwards for leg flexion MI. Focusing on training sessions, the preparation period in each trial was 2s followed by MI period lasting 4s.

The Ferrero et al.'s paper [55] shows a lower-limb motor imagery BCI that

has been designed to control a treadmill. The aim of this work is to design a lower-limb motor imagery BCI to control a treadmill and test it. Two experiments were conducted. In the first one, the activation and deactivation of the treadmill was remotely executed by an operator, subjects had to perform ten trials. During each trial, they had to alternate periods of relaxation (10s), that started and finished with an acoustic sound, motor imagery of gait (10s) and regressive count (20s), but before performed the MI task the user had to wait 10s, while before perform the regressive count he had to wait at least 4s. The second experiment consist in a closed-loop trial where the treadmill was controlled by the BMI and consisted of five trials. So in this experiment there isn't a visual feedback of the MI task but the feedback is given by the moving or not of the treadmill. In [56] the aim was the developing of an asynchronous brain-computer interface (BCI)-based lower limb exoskeleton control system based on motor imagery (MI). They decoded EEG signals in real-time, allowing the users to walk forward, sit down, and stand up while wearing the exoskeleton. EEG feature vectors associated with the motor imagery were extracted from the filtered EEG signals with common spatial patterns method. Finally support vector machine was employed to address an EEG-based three-class motor imagery classification task. The experiment was composed by 10 session, each composed by 3 phases: preparation, imagination of designed action and rest. The study of Choi et al. [57] aimed to develop an intuitive gait-related motor imagery (MI)-based hybrid brain-computer interface (BCI) controller for a lower-limb exoskeleton and investigate the feasibility of the controller under a practical scenario including stand-up, gait-forward, and sit-down. The developed MI-based BCI exoskeleton control system consists of three parts, namely data acquisition, EEG signal processing, and exoskeleton control. While the subject performs

MI tasks, a signal processing algorithm extracts features and trains the offline classifier. A decoded control command is sent to the exoskeleton via a real-time online control interface. All subjects successfully completed a gait task by wearing the lower-limb exoskeleton through the developed real-time BCI controller. The BCI controller achieved a time ratio of 1.45 compared with a manual smartwatch controller. The developed system can potentially be benefit people with neurological disorders who may have difficulties operating manual control.

2.2.2 Motor execution

In the work of Sburlea et al.[58] the aim was investigate the ability of a BCI to detect the intention to walk in stroke patients from pre-movement EEG correlates. For each of the three sessions each trial was composed by two parts: relaxation and movement. Both parts had variable time lengths according to the patient needs. The relaxation part started with an auditory cue that instructed the patients to relax and reduce movements. After approximately 10s another auditory cue instructed the patients to start walking whenever they want. Patients were previously instructed to wait a couple of seconds after hearing the second auditory cue. After every twenty trials there were break intervals with a duration adjusted to the need of the patients. A session had five phases, comprising a total of an hundred trials. In another work, Sburlea et al. [59] create a protocol for the detection of pre-movement state. The experimental protocol was composed by three sessions. Each trial was composed of two parts: relaxation and self-initiated movement. In the relaxation part that lasted 10s they were asked to stop moving, relax their muscles and to fixate their eyes on a point in the middle of the screen located at the end of the stage. The beginning of the movement part was marked

by a fixation cross. The participants were previously informed that after the appearance of the fixation cross they can start walking whenever they want, but not earlier than 1.5s. The movement task was always initiated with the right leg. After each ten trials there were break intervals. In Dong Liu et al. work [60], the aim is the decoding of lower-limb movement-related cortical potentials. The experimental procol isn't base on a free body movement but is introduced a customized gait trainer where the subjects performed self-initiated ankle plantar flexion. Participants were seated in a gait trainer (the legoPress) which can mobilize the user's legs to emulate gait movement. Visual stimuli were handled with a script and provided by a monitor to the user. Each experimental session consisted of three consecutive tasks: relax and fix a cross, perform a self-paced platar flexion with the leg indicated by a directional cue and rest. The subject was instructed to perform the movement within 7s, but not early than 2s, without explicitly counting the time. Each run consisted of sixty trials, with left and right directional cues randomized and balanced inside. Finally, the work of Lopez-Lazar et al.[14], proposes a closed-loop BMI system to control an ambulatory exoskeleton without any weight or balance support—for gait rehabilitation of incomplete spinal cord injury (SCI) patients. Using a cue-guided paradigm, the electroencephalographic signals of the subjects were used to decode their gait intention and to trigger the movements of the exoskeleton. The experimental protocol consisted of familiarization sessions and BMI sessions. The familiarization sessions allowed the subjects to get used to the protocol timings and the exoskeleton movements. On these sessions, one experimenter triggered the movements of the exoskeleton manually, warning the subject before every movement. The sessions were composed of rest and movement attempt (MA) intervals. The BMI sessions were composed of trials with four inter-

vals: ”Rest”, ”Preparation”, “Movement Attempt” and ”Movement”. During the “Rest” state (5s), the subjects were not required to perform any task, but just to relax after the previous trial. After that, a low tone was played, which marked the beginning of the “Preparation” interval (3s), during which they were instructed to relax and be prepared for the upcoming cue. A high tone denoted the start of the “Movement Attempt” interval (maximum 3s), in which they were asked to attempt to move their right leg. If the BMI detected the intention to move at any time during these 3s, the system started the “Movement” interval, in which the exoskeleton controller unblocked the joints and moved for one gait cycle: one step with right leg and one with left leg (6s). Otherwise, after the 3s, a new trial started in rest state.

2.3 Thesis aim and structure

The aim of the thesis is the implementation of a calibration protocol for a BMI-driven robotic exoskeleton. The intention is to define a calibration protocol that allow to determine the pre-movement intention of the subject. Starting from an online research, I noticed that a lot of works on the BMI to control a lower limb exoskeleton use the motor imagery or ERP [61] to detect the intention to walk of the patient. To go beyond the state-of-the-art and produce a better interaction between the exoskeleton and the subject, I propose a protocol based on motor execution of stepping movement while the subject wears a powered lower-limb exoskeleton. My work has been organized in two consecutive phases: firstly, I designed and realized the experimental protocol and setup for the recording of EEG data during lower limb exoskeleton usage. Secondly, I focused on the analysis of the EEG data and the implementation of a data-driven classifier of pre-movement neural

correlates to predict the walking intention.

The thesis is structured in six chapters: Chapter 1 'Background' and Chapter 2 'Introduction' aim to provide an overview of the issues addressed in this work, to describe the landscape of the neurorehabilitation and neurorobotics and how BMI can be useful in this application. Chapter 3 'Materials and Methods' will list the tools used and describes the proposed approach. In 'Results', Chapter 4, the efficacy and performance of the processing of the EEG data collected to train a BMI will be evaluated. Finally, in Chapters 5 and 6, respectively 'Discussion' and 'Conclusions', the results obtained will be discussed and the contribution that this work has made in relation to the state-of-the-art will be highlighted.

3 | Materials and Methods

Overview

In this chapter I will describe all the flow of my work. I start with the description of the experiment. It include the description of the subjects that partecipated at the experiment, the way in which I collected the EEG signal and the description of the instrumentation that I used, i.e. the EEG cap and the exoskeleton. Then I will describe the experimental paradigm that is at the base of my thesis. First I will focus on the different phases that compose it and then I will introduce how communication takes place between the three computer needed for the experiment. After that I will introduce how I did the processing of the EEG signal collected and then how I extracted the most discriminant features of the EEG signal. Then I will speak about the three classifiers that I considered for my thesis and the different metrics that I used to evaluate the best among them. Then will be presented the method of the integration of probabilities, used to smooth the outcomes of the classifier and the ROC curve that is computed starting from the true positive rate and false positive rate computed considering different values of the smoothing factor. Finally is done a study on different possible threshold' values to discover that can give the best true-positive false-positive rate.

3.1 Experiment

3.1.1 Partecipants

Seven subjects participated voluntarily in the experiments. They were four males and three females with an average age of 24.57 ± 1.13. They did not report any neurological disease and had no movement impairments. Three of them had already experienced BMI usage. They signed an informed consent that briefly reassumed the purposes and nature of the experiment, in accordance with the principles of the declaration of Helsinki.

3.1.2 EEG acquisition

To collect the EEG signals, a gel-based EEG cap, the wavenguard^{TM} original (ANT Neuro, Netherlands) with 64 channels was employed. The cap has the 10 - 20 distribution of the international system. All the 64 electrodes record the brain activity at 512 Hz, except one that is used for the electrooculogram (EOG) recording, that measures the ocular bio-signal when the eyes move. The CPz electrode is the reference electrode while the AFz channel is the ground. The EEG cap was linked to eego^{TM}sports mobile amplifier (ANT Neuro, Hengelo, Netherlands). This EEG technology was specifically chosen because of the active shielding of both waveguard cap electrodes and amplifier, which deliver data with good quality and protect the signal from external disturbances (e.g., power line noise, electromagnetic noise from the exoskeleton actuators). The frequency of signal acquisition is 512Hz and before the starting of the experiment a visual inspection of the EEG signal was done to asses the good quality of the signal recorded.

3.1.3 Exoskeleton

For the robotic part of the experiment the ALICE exoskeleton was used (Figure 3.1a). ALICE is an open-source machine designed by INDI Engineer and Design, a France-based interactive technology studio. ALICE robot was designed to provide physiotherapists a new tool to help in rehabilitation process, allowing them to reduce their workload. The exoskeleton is suitable to be used by adults and is intended to research purposes. From the mechanical point of view, ALICE is adjustable for adult patients with femur and tibia lengths between 35 and 50 cm and a pelvic width from 29 to 40 cm. ALICE has a support that can be adhered to the pelvis and two adjustable elements that adapt to the leg and tibia. Moreover, ALICE includes 4 active degrees of freedom (DoF), 2 for each leg, that correspond to the hip flexion-extension and the knee flexion-extension. Each joint is equipped with 2 motors and 2 linear encoders controlling the gait generation [62, 63]. The software to control ALICE exoskeleton is a closed-loop system that can reproduce the kinematic of the human walking. To make the ALICE exoskeleton works it must be powered by a battery and connected with the low-level control system that is an ArduinoMega board. It is worth noticing that the exoskeleton has no self-balancing capabilities, thus and external support system –a walker– needs to be used for stabilization (Figure 3.1b).

3.2 Experimental paradigm

All the experiments took place at Intelligence Autonomous Systems LAB of Padova University. As in [14], this session was composed by an initial period of 'Familiarization', in which the partecipant familiarizes with the exoskeleton and the walker. Then, the experiment consisted of 5 runs in which the subject

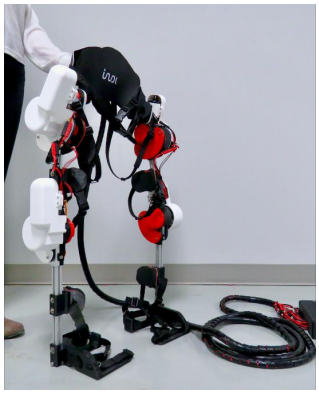

(a)

(b)

Figure 3.1: Alice exoskeleton (a), Walker (b)

made 8 step trials for each leg (16 steps in total per run). At the end of each run there was a variable period of break to avoid fatigue and/or abituation. The first thing to do is the preparation of the strumentation and of the subject. I measured subject's thigh and shank, because I need to adjust the exoskeleton's dimension to that of the subject. After that the subject was seated and wore the EEG cap with due precautions. All the electrodes were filled with the conductive gel. The quality of the EEG signal acquisition was visually verified. After that the subject wore the exoskeleton and the experimental protocol started. In the 'Familiarization' session, an operator controlled the exoskeleton and the subject had to follow the robot movement (in this phase no EEG signal was collected). Then, start the second part, i.e the 'Acquisition'. For each of the 5 runs, the paradigm was the following (Figure 3.2):

- Fixation: the subject fixes a white cross on the screen for 4s;
- Cue right leg: a violet circle appears on the screen. The subject was instructed to start the movement of the leg after approximatly 2 s fol-

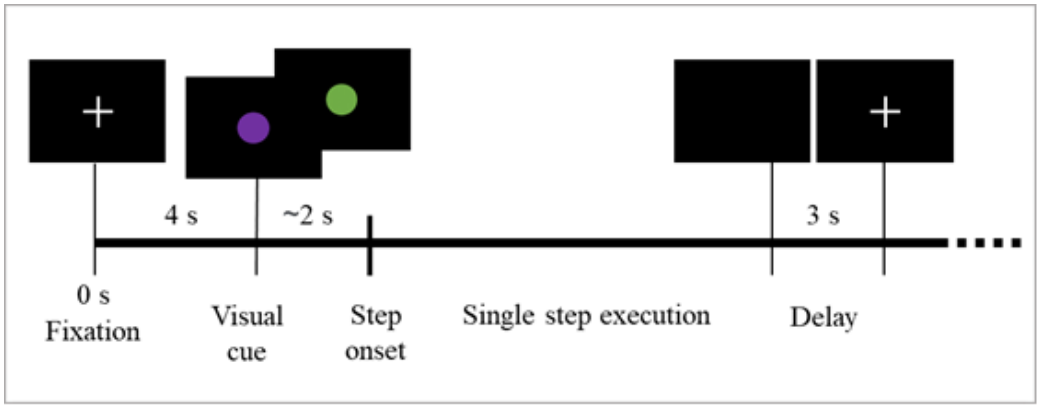

(a)

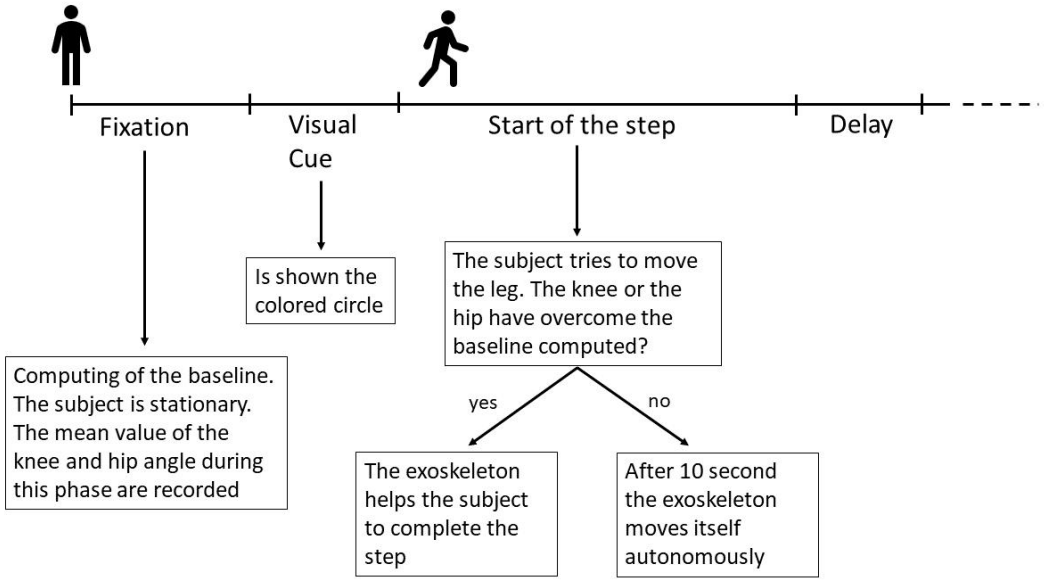

(b)

Figure 3.2: Experimental paradigm from PC GUI point of view (a), and subject point of view (b)

lowing the cue appearance, so to ensure that the movement generation was self-paced. As explained in 3.1.4, if the movement overcomes the baseline computed during fixation period then the exoskeleton receives the command to help the subject in taking the step, otherwise after 10

s from the appearance of the cue circle the exoskeleton starts moving by itself;

- Delay: after the movement of the leg there are a 3 s of black screen in which the subject can stabilize himself and retrieve the balance;

- Fixation: other 4 s of fixation;

- Cue left leg: this time the color of the cirle is green except for the eighth step of the left leg in which the color of the circle is red, to indicate that it is the last step and to allow the subject to arrive in the stand position;

- Delay: as previous.

3.2.1 Setup

The experimental setup consists of three modules: robotic exoskeleton, EEG system and graphical interface. For the proper conduct of the experiment I need to create a Robot Operating System (ROS) architecture that connects the three modules that where implemented in three laptops and connected using the ROS communication infrastructure (Figure 3.3): (i) a PC MASTER, connected to the ArduinoMega board and that sends the commands to control the exoskeleton movements; (ii) a laptop connected to the EEG acquisition system (PC EEG) placed on a backpack worn by the user; (iii) a laptop placed on the walker to provide a visual feedback of the protocol to the user through a graphical user interface (PC GUI).

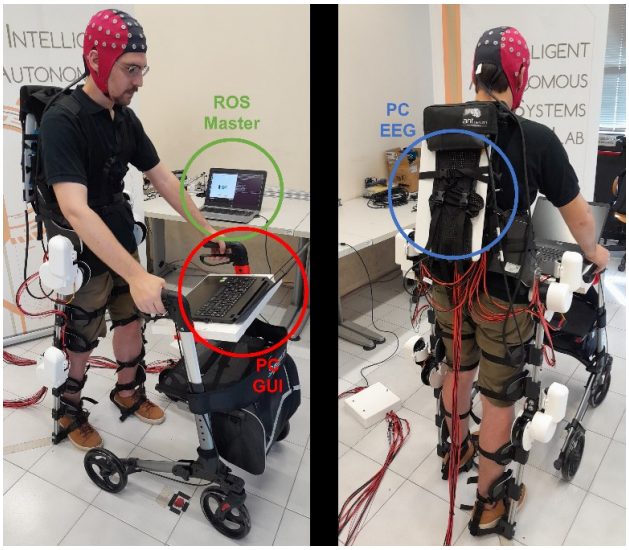

(a)

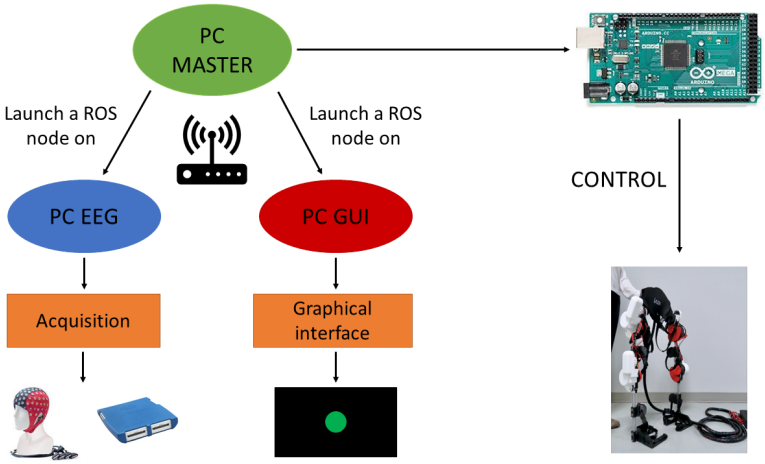

(b)

Figure 3.3: Experimental setup

PC MASTER

The PC MASTER is the one that control the exoskeleton movement but also manage the communication with the other two laptops. This PC MASTER is also the ROS Master of the ROS architecture. The ROS Master provides naming and registration services to the rest of the nodes in the ROS sys-

tem. It tracks publishers and subscribers to topics as well as services. The role of the Master is to enable individual ROS nodes to locate one another. Once these nodes have located each other, they communicate with each other peer-to-peer. The Master also provides the parameters to the server. The communication between the three PC used in the experiment is done thanks to the ROS-Neuro architecture [64]. Robot Operating System (ROS)-Neuro is an open-source framework for neurorobotic applications based on ROS. ROS-Neuro has been designed to represent the first open-source neurorobotic middleware that places human neural interfaces and robotic systems at the same conceptual and implementation level. ROS-Neuro provides several standard interfaces to acquire neurophysiological signals from different commercial devices to process EEG and EMG signals with traditional methods and to classify data with common machine learning algorithms. As in the case of ROS, the aim of ROS-Neuro is to allow the development of neurorobotic applications among different research groups as well as the possibility to easily compare heterogeneous methodological approaches and to rely and evaluate solutions proposed by others. This is guaranteed by its multi-process architecture where several stand-alone executables can coexist and can communicate through the provided network infrastructure.

About the control of the exoskeleton the first thing I had done was find a possible interaction between the ROS-Neuro architecture and the Arduino board (Figure 3.3b). This because I need to know the joint's position of exoskeleton and based on these measures I will understand if the subject is starting the gait. This idea is implemented thanks to a ROS publisher that continuosly publishes the value of the four joints' angle. During the 'Fixation' period of the paradigm is computed a baseline value based on the angles' values pubblished. During the 'Cue' period the subject will try to

move and when the hip joint angle or the knee joint angle of the leg that the subject is trying to move overcome the baseline, the exoskeleton receives a command that permits its to guide the subject to the complete of the gait movement (Figure 3.2b). This command wasn't initially implemented in the ALICE exoskeleton software. To make this possibile I created a ROS server on Arduino. The server communicates with the client placed on the ROS MASTER's node, that basing on the angles' joints value and on the leg that will be moved, will send a command to the server. This information will be taken by the server and passed to the callback function. This function will control the motors of the exoskeleton's joints and will make the gait movement possible. After the creation of all of these links, that due to the fact that there are very few works on ROS with Arduino and their connections, it took me a lot of time, I need to create the ROS network that will permit at the MASTER PC to launch ROS nodes on the two SLAVE PCs. To make the network works the three laptops must be connected to the same wifi and with the use of the SSH protocol the MASTER will know the private and the public key of the two SLAVE laptops (Figure 3.3b). Finally I need to modify the launcher file, that will be launch by the MASTER, where is indicated for each SLAVE laptop the node needed. When all the setup of the ROS MASTER laptop is finished, with the only execution of the launcher file all the ROS network will work and the protocol can start.

PC EEG

As shown in Figure 3.3 the PC EEG during the experiment is placed on the subject's backpack. Besides this pc in the backpack there is also the ANTNEURO eego^{TM}sports mobile amplifier. The wavenguard^{TM}original cap with 64 electrodes is connected at the amplifier which in turn is connected

to the laptop. When the experimental protocol start, the ROS MASTER will launch the 'ROS-NEURO ACQUISITION' and 'ROS-NEURO RECORDER' [64] nodes on the PC EEG which makes the ANTNEURO acquisition system work. The EEG signal acquired will be saved on the laptop and subsequently will be processed for creating the movement intention classifier.

PC GUI

Finally I need to create a Graphical User Interface (GUI) to give at the subject the information needed for the experiment. I created a Phython script that allow to appear a white cross for the 'Fixation' part, a violet circle for the 'CUE' of the right leg, a green circle for the 'CUE' of the left leg, and for the last step with the left leg a red circle. As it is possible to see in Figure 3.3 the PC GUI during the experiment is placed on the walker, this to allow the user to see easily the graphical interface.

3.3 Data acquisition

Even if the Antneuro cap is provided with 64 electrodes [65], I decided to focus principally on the central 27 electrodes (the CPz electrode isn't considered because is used as reference) (Figure 3.4). So the considered channels are: FC5, FC1, FC2, FC6, C3, CZ, C4, CP5, CP1, CP2, CP6, P3, PZ, P4, FC3, FCZ, FC4, C5, C1, C2, C6, CP3, CP4, P5, P1, P2, P6. The data was acquired with a frequency of 512 Hz.

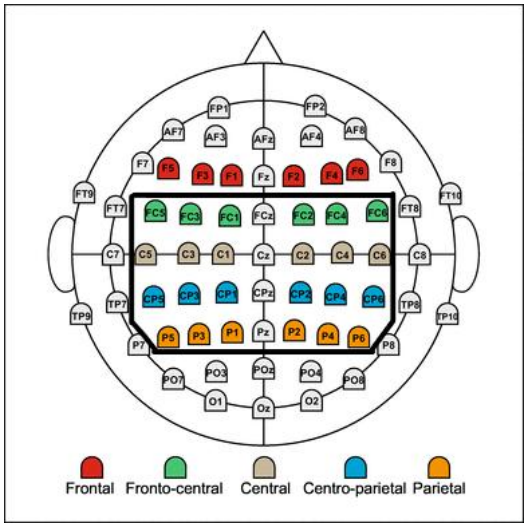

Figure 3.4: 27 selectioned electrodes

3.4 Data analysis

The data collected for each run was saved in the PC EEG in a .gdf extension. This type of data are composed by the signal acquired and some information about that signal, as the sample rate and the 'event' of the signal acquired that is important to extract relevant information from the EEG data. For example is possible to extract the type, the duration and the position of the data. The type indicates at which phase of the paradigm that part of the signal belong, the duration indicates how long it lasts and finally the position indicates when it happens. This extraction of the 'event' is possible thanks to the interaction with ROS.

3.4.1 Processing

The first thing I did to the data acquired is the application of an independent spatial filters, the small laplacian. The Laplacian method calculates for each electrode location the second derivative of the instantaneous spatial voltage

distribution, and thereby emphasizes activity originating in radial sources immediately below the electrode. Thus, it is a high-pass spatial filter that accentuates localized activity and reduces more diffuse activity [66]. The laplacian mask is obtained by subtracting the mean activity of the neighbours of each electrode:

$$e_i{}^{LAP} = e_i - \sum_{j \in S_i} h_{ij} \times e_j \tag{3.1}$$

where

$$h_{ij} = \frac{\frac{1}{d_{ij}}}{\sum_{j \in S_i} \frac{1}{d_{ij}}}$$

where e_i is the raw signal of electrode i, S_i are the neighbours of electrode i and finally d_{ij} is the distance between the pair of electrodes (i,j). This filter is data independent but also time independent. It just do linear transform of the signal and so it could be represented in matrix vector form. It can be directly applied in online BMI processing thanks to the independence with time. I manually created and applied the laplacian mask, in fact $filtered\ signal = signal \times lap$ where lap is the laplacian mask created. This filter allow us to augment the spatial distribution and a consequence is also the removal of a little part of muscular artifact [67].

3.4.2 Power Spectral Density and event-related desynchronization

After this pre - processing of the signal I computed the power spectral density. The power spectral density (PSD) refers to the spectral energy distribution that would be found per unit time, since the total energy of such a signal over all time would generally be infinite. I computed the PSD with the Welch method [68]. The Welch method takes a window of the signal and

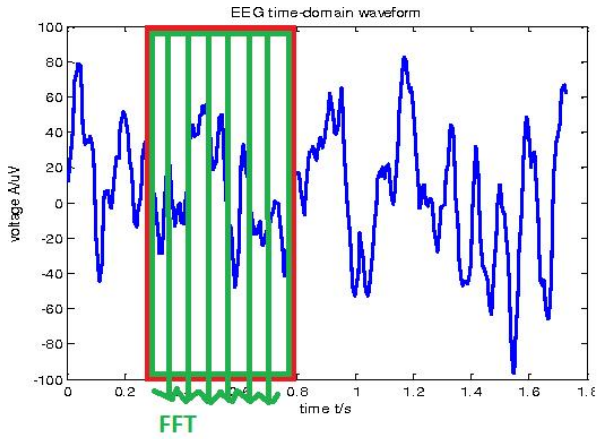

(a)

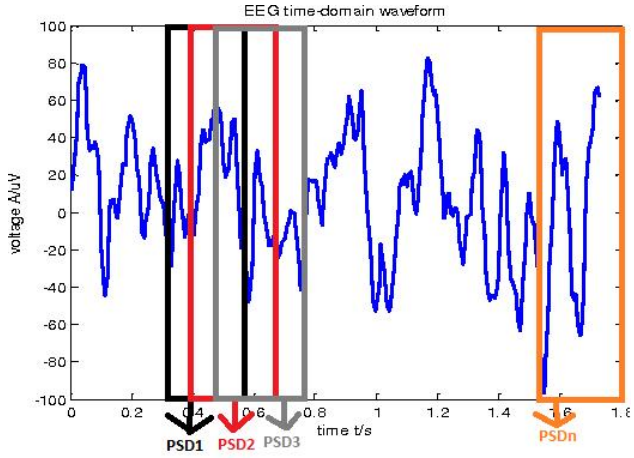

(b)

Figure 3.5: FFT on Welch method (a), PSD computed with Welch method (b)

then it splits the window into overlapping segments. Then, for each of these segments it computes the Fast Fourier Transform (FFT) of the signal and then it applies a windowing in order to remove the border effect (Figure 3.5a). Finally, it averages all the values computed for each sub - window to obtain the whole spectrum associated to a specific instant of time. From the practical point of view, at the end of computation I obtain a 3D matrix organized as $window \times frequency \times channel$ that is shifted over the whole

acquisition period (Figure 3.5b). I used as the size of the outer window (wlength) 0.5 s, the shift applied to the outer window (wshift) is 0.0625 s and I used 0.25 s as the shift of the inner segment (pshift).

To detect the ERD related to movement execution, I divided each trial into an activity period and a reference period. The reference period, called also baseline, was 1 s before the appearance of the circle that represents the cue, while as activity period I considered a window of 1 s before the onset of the movement, in order to predict the movement intention before its execution. The computing of ERD is done in this way:

$$ERD_{\%} = 100 \times \frac{A - R}{R} \tag{3.2}$$

where the letter A is referred to the activity of the signal during the activity period while R represent the reference period.

3.4.3 Features selection

After computing the PSD I needed to find a way to select the more discriminant features, which allowed us to create a good classifier for the detection of the pre-movement state.

In order to classify the EEG signal I need to extract the most informative feature from the EEG signal that is discriminant for that specific task. In motor imagery and motor execution the power of the signal is discriminant for different task. This feature is made up of amplitude, phase, and other information. More in general features can rely on different domains as instance: temporal, spatial, frequency or combination of those. In my case I considered the temporal-frequency domain, because my features were the values of PSD. Initially I thought to use a manual method for the selection

of the features. This consisted in the computing of the Fisher Score and the manual selection of the features thanks to the features map. The Fisher Score computes the distance between the distributions of two classes, in my case they were the fixation and the pre-movement class. With the Fisher Score values I created the Fisher Score matrix, that is represented with the symbol F and it is defined by observations $\times$ features. In fact the rows of this matrix is the so-called observations which are usually windows or samples while the columns are the different features that I take in consideration; in my case I used the PSD so the observations were the windows while a feature was a combination of channel $\times$ frequency. For each run, I had to compute the Fisher Score for each feature k, so:

$$FS(k) = \frac{|\,\mu_{C_1}(k) \,-\, \mu_{C_2}(k)\,|}{\sqrt{\sigma^2_{C_1}(k) \,+\, \sigma^2_{C_2}(k)}} \tag{3.3}$$

Finally I computed a features map with the mean value of the Fisher Score matrix of each run. From this last map I could identify the most discriminant features and then I selected them, considering also if the features was stable over the runs. I also tried to select the features automatically thanks to the Common Spatial Pattern (CSP) [69]. The CSP is a mathematical procedure that finds a spatial filter to project EEG segments onto a space so that its variance from one class is maximized while that from another class is minimized. For the analysis, the raw EEG data of a single trial is represented as an $N \times T$ matrix E , where N is the number of channels (i.e., recording electrodes) and T is the number of samples per channel. With the CSP is found a projection matrix W that give the decomposition of a trial matrix E in such a way : $Z = WE$, where the columns of $W^{-}1$ are the common spatial patterns and can be seen as time-invariant EEG source distribution

vectors. In my procedure I decided to apply the CSP to all the PSD data of fixation and pre-movement concatenated for each trial and I didn't divide it basing on the run. This because the CSP works better with a bigger sample size. After the application of CSP, I selected the best pattern-frequency pairs applying again the Fisher Score on the CSP-projected EEG data.

3.4.4 Classifiers

To identify the best classification pipeline, I tested three machine learning models that are commonly employed in BMI. All the classifiers have been trained and evaluated with a 5-fold cross-validation procedure with the previously extracted features from each subject. Their performance have been compared considering the average sample-by-sample accuracy and loss on the validation folds.

Linear Discriminant Analysis (LDA)

Linear discriminant analysis (LDA) or discriminant function analysis is a generalization of Fisher's linear discriminant, a method used in statistics and other fields, to find a linear combination of features that characterizes or separates two or more classes of objects or events. The resulting combination may be used as a linear classifier, or, more commonly, for dimensionality reduction before later classification [70]. LDA focuses primarily on projecting the features in higher dimension space to lower dimensions. It can achieve this in three steps:

- Firstly, it needs to calculate the separability between classes which is the distance between the mean of different classes. This is called the between-class variance (S_b).

- Secondly, it calculates the distance between the mean and sample of each class. It is also called the within-class variance (S_w).

- Finally, it constructs the lower-dimensional space which maximizes the between-class variance and minimizes the within-class variance. P is considered as the lower-dimensional space projection, also called Fisher's criterion.

$$P_{LDA} = \underset{P}{\operatorname{argmax}} \frac{|P^T S_b P|}{|P^T S_w P|} \tag{3.4}$$

The representation of LDA is pretty straight-forward. The model consists of the statistical properties of its data that has been calculated for each class. Predictions are made by providing the statistical properties into the LDA equation. The properties are estimated from the data. Finally, the model values are saved to file to create the LDA model. The assumptions made by an LDA model about the data are that each variable in the data is shaped in the form of a bell curve when plotted, i.e. Gaussian, and that the values of each variable vary around the mean by the same amount on the average, i.e. each attribute has the same variance. The LDA model is able to estimate the mean and variance from the data for each class with the help of these assumptions. LDA models uses Bayes' Theorem [71] to estimate probabilities. They make predictions based upon the probability that a new input dataset belongs to each class. The class which has the highest probability is considered the output class and then the LDA makes a prediction.

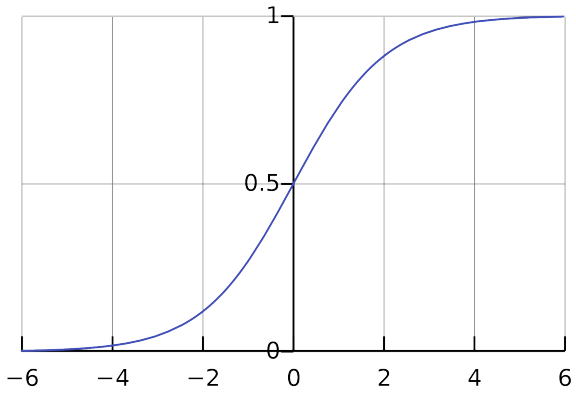

Figure 3.6: Logistic Regression function

Logistic Regression (LR)

Logistic Regression is a powerful supervised machine learning algorithm used for binary classification problems. The best way to think about LR is that it is a linear regression but for classification problems. Logistic Regression essentially uses a logistic function defined below to model a binary output variable [72]. The Logistic Regression's range is bounded between 0 and 1, in addition does not require a linear relationship between inputs and output variables. This is due to applying a nonlinear log transformation to the odds ratio:

$$Logistic\ function = \frac{1}{1 + e^{-}x} \tag{3.5}$$

where x is the input variable. LR uses a loss function referred to as "maximum likelihood estimation (MLE)" which is a conditional probability. If the probability is greater than 0.5, the predictions will be classified as class 0. Otherwise, class 1 will be assigned. In Figure 3.6 is possible to see the functioning of logistic regression function.

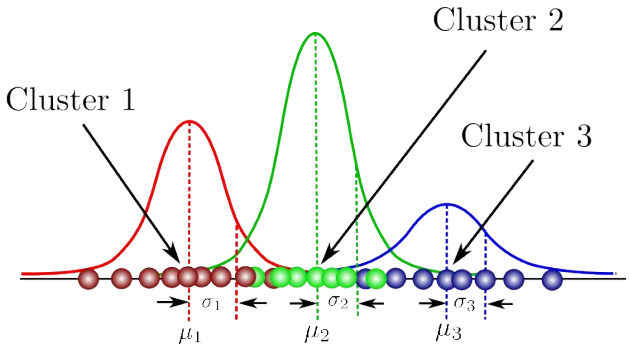

Figure 3.7: Gaussian distribution

Supervised Gaussian Mixture Model (SGMM)

A Gaussian Mixture is a function that is comprised of several Gaussians, each identified by $k \in 1, \ldots, K$, where K is the number of clusters in which the dataset is divided. Each Gaussian k in the mixture is comprised of the following parameters:

- A mean μ that defines its centre;
- A covariance Σ that defines its width. This would be equivalent to the dimensions of an ellipsoid in a multivariate scenario;
- A mixing probability π that defines how big or small the Gaussian function will be.

In Figure 3.7 there are three Gaussian functions, hence K = 3. Each Gaussian explains the data contained in each of the three clusters available. The mixing coefficients are themselves probabilities and must meet this condition:

$$\sum_{k=1}^{K} \pi_k = 1 \tag{3.6}$$

To determine the optimal values for these parameters it must ensure that each Gaussian fits the data points belonging to each cluster. This is exactly

what maximum likelihood does. In general, the Gaussian density function is given by:

$$N(x|\mu,\Sigma) = \frac{1}{(2\pi)^{D/2}|\Sigma|^{1/2}} \exp(-\frac{1}{2}(x - \mu)^T \Sigma^{-1} (x - \mu)) \tag{3.7}$$

Where x represents its data points, D is the number of dimensions of each data point, μ and Σ are the mean and covariance. Could also be useful to take the log of this equation, which is given by:

$$ln\, N(x|\mu,\Sigma) = -\frac{D}{2} ln(2\pi) - \frac{1}{2} ln(\Sigma) - \frac{1}{2}(x - \mu)^T \Sigma^{-1} (x - \mu) \tag{3.8}$$

If this equation is differentiated with respect to the mean and covariance and then equate it to zero, then it will be able to find the optimal values for these parameters, and the solutions will correspond to the Maximum Likelihood Estimates (MLE) for this setting. But the traditional Gaussian Mixture Model (GMM) is an unsupervised learning method. The parameters in the model are derived only by the training samples in one class without taking into account the effect of sample distributions of other classes, hence, its recognition accuracy is not ideal sometimes. In [73] is presented an approach for estimating the parameters in GMM in a supervising way. The supervised Gaussian Mixture Model (sGMM) improves the recognition accuracy of the GMM.

3.4.5 Performance metrics

To understand the performance of the classifiers I need to estimate the accuracy, the total error rate (the misclassified also known as the one classified wrongly) and the test on new data not used for the training. The problem that a classifier solves is to assign to a specific belonging class one specific

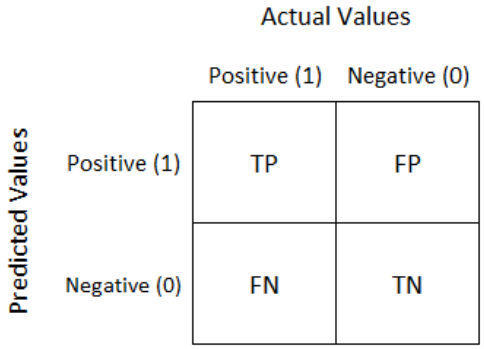

Figure 3.8: Confusion matrix

vector of features, representative of the phenomenon analysed. So, one observation x could be assign to a specific true class represent in our mathematical analysis as y. In my case I used a binary classification, so the class considered are 2, the fixation, which label was 0, and the pre-movement, which label was 1. To evaluate the goodness of the results obtained with the classifier chosen I computed the confusion matrix, which holds different types of information. In Figure 3.8 is reported a confusion matrix computed for a two class generic classifier. The components of this matrix are very important. In the main diagonal there is the presence of the fraction or percentage of correct classification of my classifier, while in the secondary diagonal is reported the fraction or percentage of incorrect classification output of our classifier. The elements in the main diagonal represent: in the upper left corner the probability to classify an event as positive while this one is positive, so the True Positive (TP), in the lower right corner there is the True Negative (TN), so the probability to classify an event as negative while this one is negative. The two elements in the secondary diagonal have a different meaning. The one reported in the lower left corner defines the probability to classify an event as negative while this one is positive, so this is the False

Negative (FN), while the element reported in the upper right corner could be interpreted vice versa, so the probability to classify an event as positive while this one is negative, so this is the False Positive (FP). In general, in a classification problem the main problem is to maximize the content of the main diagonal and minimize the content in the secondary diagonal. Usually, prefer to have more false positive of more false negative or vice versa is application dependent. To quantify the goodness of the classifier or the model it has been introduced other two important indexes, the sensitivity, and the specificity.

$$Sensitivity = \frac{True\ Positive}{All\ Positive} = \frac{TP}{TP + FN} \tag{3.9}$$

$$Specificity = \frac{True\ Negative}{All\ Negative} = \frac{TN}{TN + FP} \tag{3.10}$$

These are two important metrics. Generally, the sensitivity and the specificity are inverse related one from each other. In fact, as specificity increases the sensitivity decreases and so I need to find a right balance between these two terms. Another important effect of increase the specificity and sensitivity are that if I increase the specificity, and so the ability to classify negative an event I would also increase indirectly the false negative rate, and this will decrease the sensitivity. Vice versa, if I increase too much the sensitivity, I will increase the possibility to classify correct a result, but this will lead to an increase of the false positive fraction. Another important metric to quantify the goodness of the classifier is the accuracy. Classification accuracy is a metric that summarizes the performance of a classification model as the number of correct predictions divided by the total number of predictions. It is easy to calculate and intuitive to understand, making it the most common

metric used for evaluating classifier models.

$$Accuracy = \frac{Number\,of\,correct\,predictions}{Total\,number\,of\,predictions}$$

and in the case of a binary classifier is possible to compute the accuracy with the terms used in the confusion matrix:

$$Accuracy = \frac{TP + TN}{TP + TN + FP + FN} \tag{3.11}$$

One problem of the accuracy is that isn't considered how much strong is the choice done, so a sample that is near the threshold is considered as the same as a sample that strongly belong to a class, i.e a sample with a probability of 0.45 weighs the same as a sample that belong to the class 0 with a probability of 0.2. To consider also this fact I also introduce the cross-entropy loss. Cross-entropy loss, or log loss, measures the performance of a classification model whose output is a probability value between 0 and 1. Cross-entropy loss increases as the predicted probability diverges from the actual label. In a binary classification the cross-entropy can be calculated as:

$$c.e.\,loss = \frac{1}{N} \times \sum_{i=1}^{N} -\left[y_i\,log(p_i) + (1 - y_i)\,log(1 - p_i)\right] \tag{3.12}$$

where N is the number of observations, y is the binary indicator of the considered observation i and p is the associated probability. A smaller cross-entropy loss value indicate a better classification. Basing on this, I considered as indicator for the best classifier the cross-entropy loss. I decided to test three classifiers: Linear Discriminant Analysis (LDA), Logistic Regression (LR) and a Supervised Gaussian Mixture Model (SGMM). The different classifiers were tested on the training dataset and the prediction was done on the vali-

dation dataset. The division in training ad validation was performed starting from the PSD fixation and pre-movement data and applying a k-fold cross validation, with k=5. This allowed to test each classifier k-times and I took the predicted probabilities that gave the smallest cross-entropy loss value. It is important to notice that I considered a trial based approach, so the sample of the same trial can't be divided in training and validation, but all the sample of the same trial or belong to the training set or to the validation set. Each classifier gives me two different type of data that are linked one to each other:

- Predicted probabilities: indicates the probabilities that a sample have to belong to one class or the other;
- Predicted label: indicates the class at which the classifier assigned the sample.

The predicted label given by the selectioned classifier was compared to the real class label, that thanks to a priori knowledge contains the real belonging class of each sample. This comparison allowed me to compute the accuracy and the cross-entropy loss for each of the 5 folds. At the end I decided to take the classifier that in mean gave the lesser cross-entropy loss.

3.4.6 Integration of probabilities and ROC curve

As presented in [74], in order to smooth the outcomes of the classifier an exponential integrator has been used to accumulate the evidence over time with the following decision making formula:

$$D(y_t) = \alpha \times D(y_t - 1) + (1 - \alpha) \times p(y_t \mid x_t) \tag{3.13}$$

where $D(y_t)$ is the current level of decision making and α $(0 < \alpha < 1)$ is the integration parameter, called also smoothing factor. Smaller values of α actually reduce the level of smoothing, and in the limiting case with $\alpha = 0$ the output series is just the current observation. Values of α close to zero have less of a smoothing effect and give greater weight to recent changes in the data, while values of α closer to one have a greater smoothing effect and are less responsive to recent change. This exponential smoothing for the accumulation of the probabilities was applied at each trial of the validation set. The idea of this approach was to find a good threshold that allowed me to better classify a trial as true positive, i.e trial that I know is a pre-movement trial and is classified as pre-movement trial, or as false negative, i.e trial that I know is a fixation trial and is classified as fixation trial. In fact if the actual decision probability $D(y_t)$ overcomes the threshold the trial is classified as pre-movement, otherwise is considered a fixation trial.
The problem of this approach is that I have two degree of freedom, one is

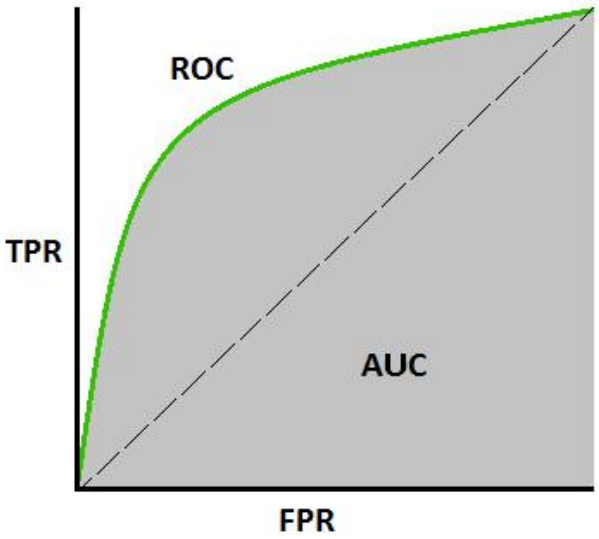

Figure 3.9: ROC curve and AUC

the smoothing factor α, the other is the threshold. To solve this, I used the following method:

1. Creation of a vector with different values of smoothing factor α. In my case I test the following values: [0.98, 0.96, 0.94, 0.92, 0.90, 0.88, 0.86, 0.84, 0.82, 0.80, 0.75, 0.7, 0.65, 0.6, 0.55, 0.5, 0.4];

2. Creation of a vector with different values of the threshold. In my case I test the following values: [0.75, 0.7, 0.65, 0.6, 0.55, 0.5, 0.45, 0.4, 0.35, 0.3, 0.25, 0.2];

3. Creation of a table with the values of TP rate and FP rate for each combination between α and threshold;

4. For each value of α, create a ROC curve and compute the area under the curve (AUC);

5. Choose the best smoothing factor α, i.e the one that gives the bigger AUC. In the case of more α take the bigger one.

A receiver operating characteristic curve, or ROC curve , is a graphical plot that illustrates the diagnostic ability of a binary classifier system as its discrimination threshold is varied [75]. The ROC curve is created by plotting the true positive rate (TPR) against the false positive rate (FPR) computed with different values of the threshold (Figure 3.9). It is usually used in BMI protocol to compare the results of different classification sessions [54]. Considering the best α for each subject, I considered for each of them the mean accumulation of probabilities, both for fixation and pre-movement, computed by averaging the different trials. Starting from this I considered a 'mean subject'. This ideal subject had the accumulated probabilities of fixation and pre-movement that correspond to the the mean values of that of the others

subject. After the choice of the best smoothing factor, so the reduction of the degrees of freedom from two to one, I analyzed the threshold. The idea was to find the best threshold for each subject, so the threshold that can maximize the rate between the true positive and the false positive. This because higher is the rate and higher is the probability to define a pre-movement trial as such, and so at the same time the probability to take a fixation trial as pre-movement trial will be very small. Notice that I considered only the case where the TP rate where bigger than the 65% of the case.

4 | Results

4.1 Acquisition

Due to the high temperature in the lab, the subject S.04 and S.05, didn't complete all the run provided by the experimental protocol, but I had only 3 runs for the subject S.04 and 2 runs for the subject S.05

4.2 Event-related desynchronisation

In Figure 4.1 there is the PSD ERD average map for the subject 01, focusing on Cz and FCz channels since the lower limb are mostly represented in the central area of the motor cortex. In the Figure 4.1 is seen a good desynchronization, marked by deep blue zone, approximately 1 s before the movement onset (occuring at 0 s).

4.3 Fisher Score map

For each subject I computed two Fisher Score matrices, one with the use of the CSP decomposition and one with the data in the channel domain. For both cases, I principally focused on the α (8Hz - 12Hz) and β (13 Hz - 30Hz) band, but sometimes I considered also the frequencies between the 4Hz and

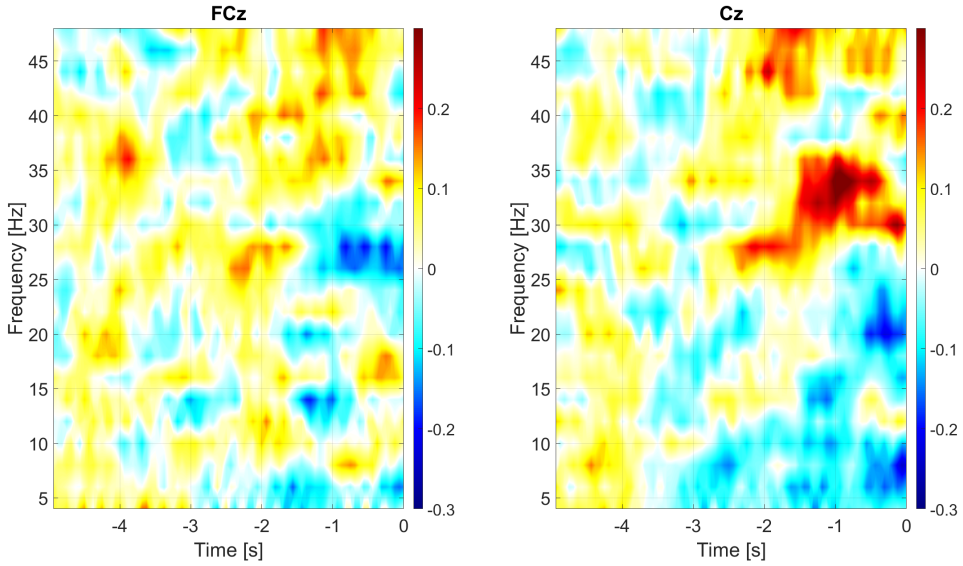

Figure 4.1: ERD map of subject 01. For the computing was considered all the data of all the S.01 files.

8Hz if a feature in that range shows a discriminancy.

In Figure 4.2 are shown the features maps for the subject 01. The top map has the frequency on the x-axis and the channels on the y-axis, while bottom one has the frequency on the x-axis and the common patterns on the y-axis. Is shown how the CSP works in a good case: the decomposition allow to better divide the classes, bringing to a graph in which the more discriminant patterns are the first or the last, while in the middle there are principally non discriminant features. In Additional files the features map of all the subjects are provided.

For both the cases, I decided to take the 6 most discriminant features, and if there were more than 6, I took the ones that show more consistency over the runs. Table 4.1 shows the features selectioned for each subject in the case without CSP, while in Table 4.2 there are the features selectioned in the case with CSP. Finally, in Figure 4.3 are shown the more present frequencies that

characterize the selected features in the case without CSP, while in Figure 4.4 that with CSP.

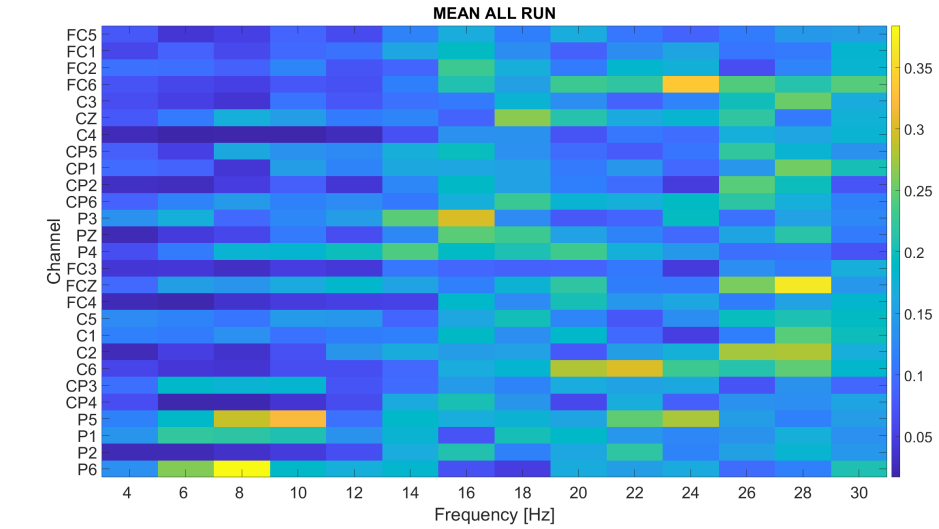

(a)

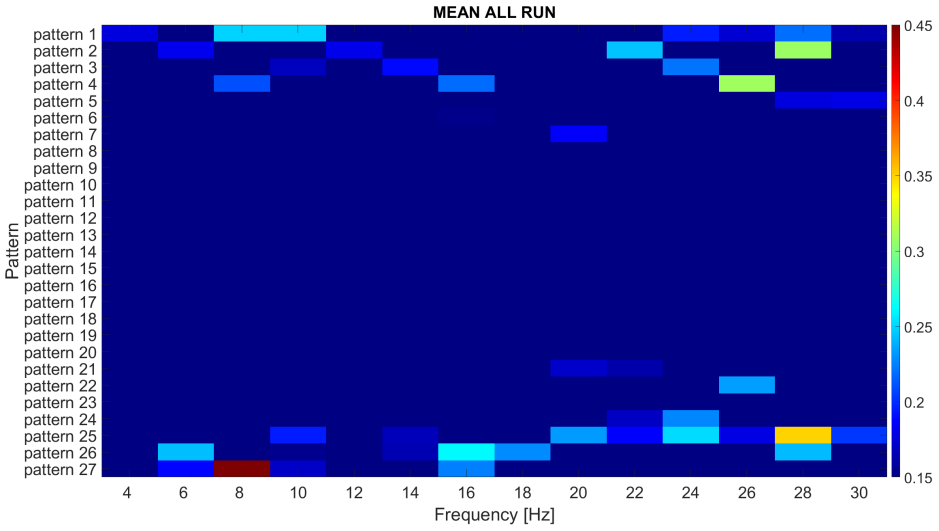

(b)

Figure 4.2: Features map S.01 (a), Features map CSP S.01 (b)

Subject	Features normal case					
S.01	8Hz - P6	10Hz - P5	16Hz - P3	20Hz - C6	24Hz - FC6	28Hz - FCz
S.02	10Hz - P4	10Hz - P2	16Hz - P5	16Hz - C3	18Hz - FC1	18Hz - CP3
S.03	4Hz - FCz	6Hz - FCz	14Hz - P5	16Hz - C1	18Hz - FC6	26Hz - P4
S.04	8Hz - C3	8Hz - P3	12Hz - FC5	16Hz - C3	20Hz - FC6z	24Hz - CP5
S.05	8Hz - P3	12Hz - P5	14Hz - FC3	18Hz - CP6	20Hz - CP5	28Hz - C6
S.06	6Hz - C1	14Hz - FC1	16Hz - FC3	22Hz - C5	24Hz - Pz	30Hz - P6
S.07	6Hz - FCz	14Hz - C2	16Hz - FC6	22Hz - Cz	26Hz - FC6	28Hz - FC2

Table 4.1: Table containing the selectioned feauteres for each subject in the case without CSP.

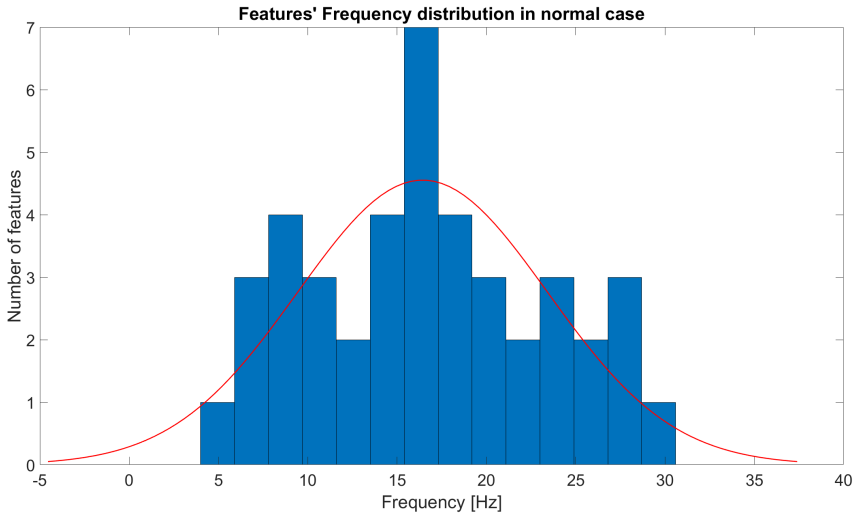

Figure 4.3: Histogram of features' frequencies in normal case

Subject	Features CSP case					
S.01	8Hz - p.27	10Hz - p.1	16Hz - p.26	26Hz - p.4	28Hz - p.2	28Hz - p.25
S.02	14Hz - p.4	18Hz - p.2	20Hz - p.1	22Hz - p.3	24Hz - p.1	24Hz - p.25
S.03	4Hz - p.27	14Hz - p.27	16Hz - p.2	28Hz - p.2	28Hz - p.22	30Hz - p.1
S.04	8Hz - p.2	10Hz - p.2	16Hz - p.5	20Hz - p.1	24Hz - p.26	28Hz - p.25
S.05	16Hz - p.27	20Hz - p.24	24Hz - p.27	26Hz - p.27	28Hz - p.27	30Hz - p.26
S.06	10Hz - p.2	14Hz - p.27	18Hz - p.1	26Hz - p.1	28Hz - p.1	30Hz - p.1
S.07	14Hz - p.2	20Hz - p.2	22Hz - p.3	24Hz - p.3	26Hz - p.26	28Hz - p.2

Table 4.2: Table containing the selectioned features for each subject in the case with CSP.

4.4 Classification

Once the best features were selected I needed to select the classifier that give the best performance.

	WITHOUT CSP				WITH CSP			
S.01	max accuracy	mean accuracy	min c.e.loss	mean c.e.loss	max accuracy	mean accuracy	min c.e.loss	mean c.e.loss
LDA	70.1172%	**65.4297%**	**0.5405**	**0.6035**	62.8906%	59.6875%	0.6265	0.6745
LR	**71.0938%**	65.3906%	0.5670	0.6264	**64.0625%**	**61.2500%**	**0.6229**	**0.6552**
sGMM	65.2344%	61.0938%	0.7178	0.9232	61.9141%	54.1016%	0.7143	1.2376

(a) Table with classifiers' values for the S.01

	WITHOUT CSP				WITH CSP			
S.02	max accuracy	mean accuracy	min c.e.loss	mean c.e.loss	max accuracy	mean accuracy	min c.e.loss	mean c.e.loss
LDA	59.3750%	53.5939%	**0.6754**	0.7008	58.0729%	46.8269%	0.6874	0.7188
LR	58.0729%	52.8646%	0.6795	**0.6919**	**61.1979%**	**47.3838%**	**0.6872**	**0.7056**
sGMM	**65.3646%**	**55.7572%**	0.6810	0.8829	50.2604%	47.2997%	0.9084	1.1700

(b) Table with classifiers' values for the S.02

	WITHOUT CSP				WITH CSP			
S.03	max accuracy	mean accuracy	min c.e.loss	mean c.e.loss	max accuracy	mean accuracy	min c.e.loss	mean c.e.loss
LDA	62.5%	59.1964%	0.637	0.6647	57.1429%	47.6339%	**0.6835**	0.7146
LR	**63.3929%**	**61.3393%**	**0.6344**	**0.6520**	**62.5000%**	**48.2143%**	0.6906	**0.7061**
sGMM	56.0268%	51.6518%	0.7007	0.8367	56.6964%	50.1339%	0.9577	1.1815

(c) Table with classifiers' values for the S.03

	WITHOUT CSP				WITH CSP			
S.04	max accuracy	mean accuracy	min c.e.loss	mean c.e.loss	max accuracy	mean accuracy	min c.e.loss	mean c.e.loss
LDA	69.6429%	**60.5580%**	0.5774	**0.6826**	51.3393%	40.5580%	0.6975	**0.7653**
LR	67.1875%	58.7054%	0.6124	0.6882	51.3393%	40.1228%	0.6980	0.7811
sGMM	**70.0893%**	58.6830%	**0.5383**	1.0420	**61.1607%**	**46.4509%**	**0.6647**	1.0997

(d) Table with classifiers' values for the S.04

	WITHOUT CSP				WITH CSP			
S.05	max accuracy	mean accuracy	min c.e.loss	mean c.e.loss	max accuracy	mean accuracy	min c.e.loss	mean c.e.loss
LDA	69.5313%	61.0938%	**0.5657**	0.6647	71.8750%	**67.9688%**	0.6569	0.6685
LR	66.4063%	60.6250%	0.5792	**0.6523**	**73.4375%**	66.7188%	0.6123	**0.6590**
sGMM	**70.0893%**	**61.5625%**	0.5742	0.9980	72.6563%	63.9063%	**0.5673**	0.9316

(e) Table with classifiers' values for the S.05

	WITHOUT CSP				WITH CSP			
S.06	max accuracy	mean accuracy	min c.e.loss	mean c.e.loss	max accuracy	mean accuracy	min c.e.loss	mean c.e.loss
LDA	67.7083%	58.1250%	**0.6325**	**0.6693**	58.3333%	51.5104%	0.6879	**0.7111**
LR	**71.0938%**	**58.8021%**	0.6478	0.6748	**61.7188%**	52.6042%	**0.6848**	0.7151
sGMM	62.2396%	57.3958%	0.7795	0.8080	60.9375%	**52.9167%**	0.8332	1.0513

(f) Table with classifiers' values for the S.06

	WITHOUT CSP				WITH CSP			
S.07	max accuracy	mean accuracy	min c.e.loss	mean c.e.loss	max accuracy	mean accuracy	min c.e.loss	mean c.e.loss
LDA	**64.8438%**	**56.7578%**	**0.6475**	**0.6825**	54.6875%	49.9219%	**0.6862**	0.6963
LR	62.5%	55.4227%	0.6755	0.6860	**55.0781%**	**50.8594%**	0.6920	**0.6930**
sGMM	56.6406%	53.9453%	1.0042	1.1396	51.7578%	50.7031%	0.8783	1.0774

(g) Table with classifiers' values for the S.07

Table 4.3: Table that summarizes the accuracy and c.e.loss values for all the subjects

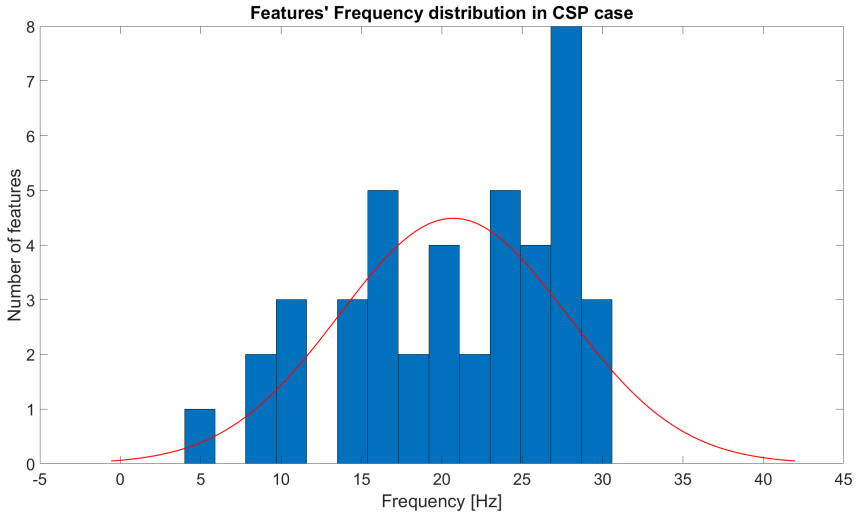

Figure 4.4: Histogram of features' frequencies in CSP case

Table 4.3 shows for each subject the performance achieved by the three tested classifiers trained with channels' domain data or CSP components. The 'max accuracy' indicates the maximum accuracy of the 5 folds, the 'mean accuracy' indicates the mean accuracy value across the folds, the 'min c.e.loss' indicates the minimum value of cross entropy loss between the 5 folds and finally the 'mean c.e.loss' indicates the mean cross entropy loss value across the folds. From these results, it can be said that on average the CSP-based classifiers achieved lower performances that the classifiers trained with data from the channels' domain. In fact, the values of the maximum accuracy and the mean accuracy for the case without CSP are larger than the case with CSP and the values of the minimum cross entropy loss and the mean cross entropy loss are smaller in the case without CSP respect the case with CSP. This can also be seen in Table 4.4, where are reported the average results across subjects of each classifier. Considering both the accuracy and the cross entropy loss, the best performance is achieved by the LDA classifier and thus it was used for the following analysis. Once the classifier was chosen,

I took the predicted probabilities and the predicted label of the fold that gave the smaller cross-entropy loss value.

WITHOUT CSP		
Classificator	mean accuracy	mean c.e. loss
LDA	59.2506% ± 3.7142	0.6669 ± 0.031
LR	59.0214% ± 4.0726	0.6674 ± 0.024
sGMM	57.1556% ± 3.6486	0.9472 ± 0.119

WITH CSP		
Classificator	mean accuracy	mean c.e. loss
LDA	52.0153% ± 9.0866	0.7070 ± 0.032
LR	52.4505% ± 8.9364	0.7022 ± 0.042
sGMM	52.2160% ± 5.8415	1.1070 ± 0.101

Table 4.4: Values of the mean subject

4.5 ROC curve

For each trial in the validation set, the outcome of the LDA classifier was accumulated using the exponential integrator of section 3.4.3. In the trials belonging to the pre-movement state, if the integrated probability overcomes the threshold, the trial is considered a TP, as the movement was correctly predicted from the EEG data, and as a FN otherwise. For the fixation trials, if the integrated probability overcomes the threshold, the trial is considered a FP, and as TN otherwise.

Table 4.5 shows the smoothing factor α selected for each subject. The selection was performed by looking to the variation of the ROC for the different values of α, as shown in Figure 4.5 for S.01.

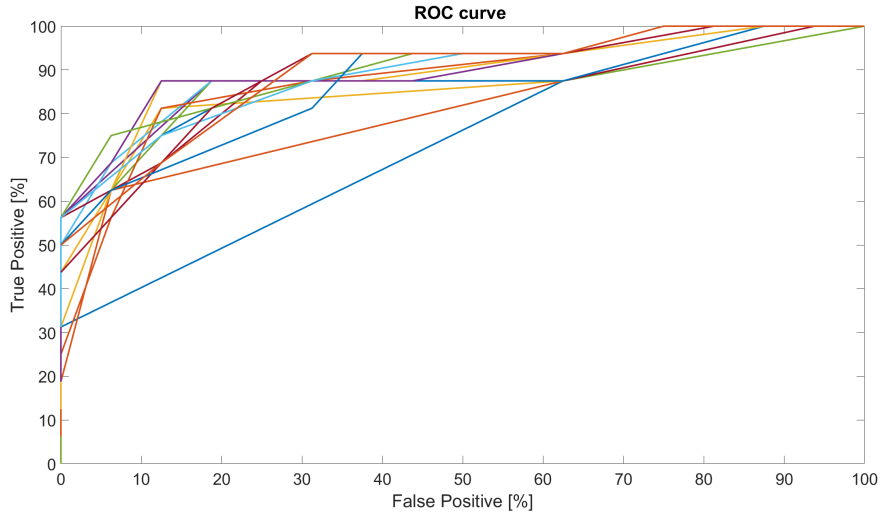

(a)

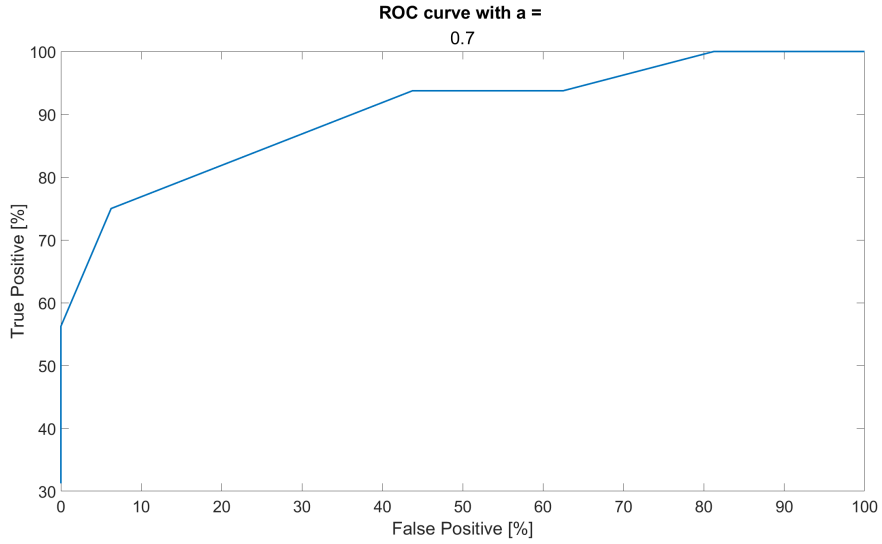

(b)

Figure 4.5: ROC curves for S.01 (a), ROC curve with the best AUC for S.01 (b)

4.5.1 Smoothing factor α

The best smoothing factor is the one that gave the bigger AUC for each subject. In Figure 4.5 and in Figures from 7.7 to 7.12 there are the different

Subject	α	AUC
S.01	0.7	0.9023
S.02	0.96	0.6746
S.03	0.82	0.6939
S.04	0.6	0.7857
S.05	0.9	0.9688
S.06	0.4	0.8229
S.07	0.94	0.7461

Table 4.5: Smoothing factor chosen for each subject and bigger AUC

ROC curves for each subject and the ROC curve with the biggest AUC, while Table 4.5 reassumes the smoothing factor that gives the biggest AUC for each subject.

4.5.2 Integration of probabilities and threshold

Subject	Threshold	TPR	FPR
S.01	0.65	75%	6.25%
S.02	0.5	66.67%	41.67%
S.03	0.55	85.71%	50%
S.04	0.55	71.43%	28.57%
S.05	0.6	75%	0%
S.06	0.6	66.67%	25%
S.07	0.5	93.75%	68.75%

Table 4.6: Threshold's best values

In Figure 4.6 is shown the grand-average of the integrated probabilities across subjects for fixation (a) and pre-movement (b) trials. To find the best threshold for each subject, I analysed and considered the threshold that maximize the ratio between the TPR and the FPR. I used a small number of possible thresholds because I wanted a linear shape of the ROC curve. If I considered more possible values of the threshold, due to the fact that there

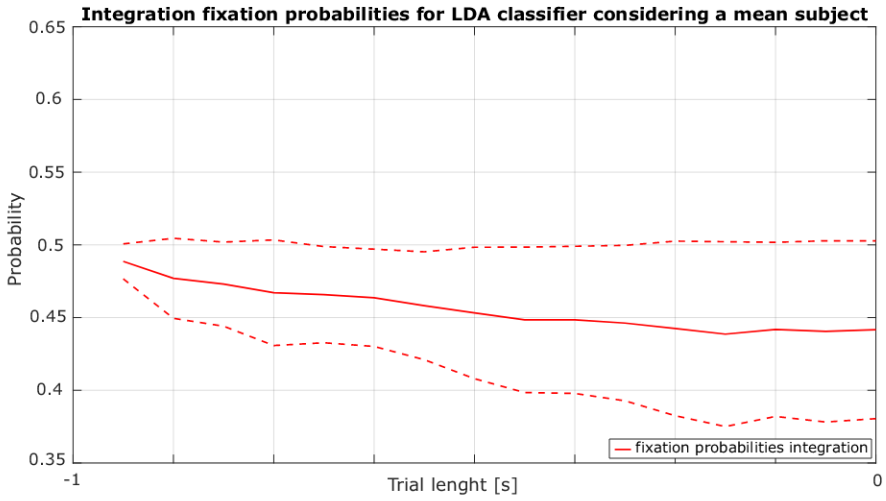

(a)

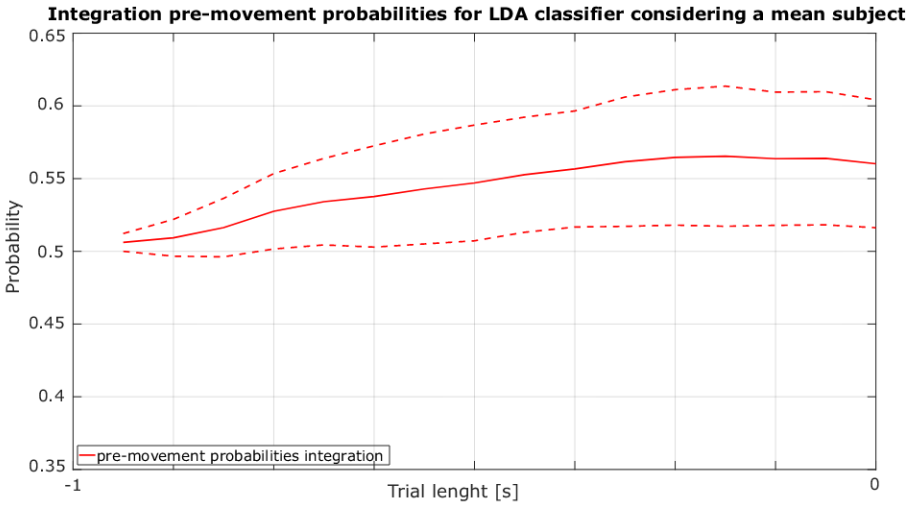

(b)

Figure 4.6: Accumulation of mean fixation probabilities (a), Accumulation of mean pre-movement probabilities (b)

are a small number of validation trials, I would have found not a linear ROC curve but a stairs ROC curve. In Figure 4.7 there is the trend of TPR and FPR at the variation of the threshold for S.01, computed with the selected smoothing factor. The results for the other subjects are reported in the

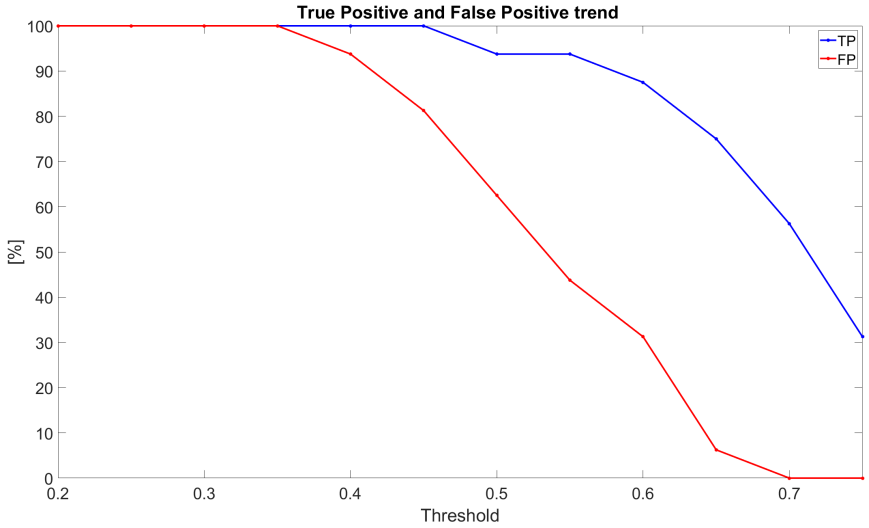

Figure 4.7: Trend of TPR and FPR of S.01

Addional Materials. In Table 4.6 is shown the best threshold selected for each subject and the corresponding TPR and FPR.

5 | Discussion

Recalling section 2.2, for the experimental protocol I took the idea of using some visual stimuli for the paradigm from [54, 60, 59] while in the other papers they used some auditory cue. About how the paradigm is structered I'm based on [14, 59] that divide a first part of relaxation/fixation and a second part of movement attempt and movement. About the timing, the number of trials and the number of runs I took some information from everyone. In Figure 4.1 is possible to see a good desynchronization, marked by deep blue zone, approximately 1 s before the movement onset. This result is expected and in line with neuroscientific literature [76], as an ERD should appear approximately from 0.3 s to 0.5 s before the starting of the movement in the brain area related to the body part interested by the movement. This feature indicates the subject's preparation to the movement. The choice of 1 s before the self-paced movement onset is also confirmed by [76], where they even consider 2 s before the movement onset. I took the same number of samples for fixation and pre-movement to have balanced classes to which apply the classifier.

The Fisher Score is a good method for the selection of the most discriminant features, and often is used in BMI based on self-paced movement or motor imagery [77]. I expected that each subject had a small number of very discriminant features and others some important features, but this happen only

for the subject 01 and 07, while for the others there were a lot of number of discriminant features, that made the selection very difficult. Instead, in the case of CSP application I found a less number of discriminant features (except for the subject 04 and 05, that are also the subjects with least number of runs), so the selection was easier. Interestingly, as shown in Figure 4.3 and Figure 4.4, the most discriminant features have been found on average in the α and β bands, strengthening the fact the BMI is effectively identifying task-related brain features and it is not significantly affected by movement-related low-frequency artifacts (e.g., cable movements) and high-frequency noise (e.g., EMG contamination).

About the classifiers I decided to use only that are supervised, because I already knew the class at which each trial belong. I used the LDA because is one of the most used in BMI to decode the user gait intention [78, 79]. The Logistic Regression and the supervised Gaussian Mixture Model are also applied because they are simple to apply and fast. I had applied the cross validation to the dataset, divided it into 5 folds, each composed by a training set and a validation set, with the training set that contained approximately the 80% of the trials. I applied each classifier at each fold and in Table 4.3 there are the best performances for each classifier. In general is possible to see that the performances in the case without CSP are better for each classifier, both in accuracy and in cross-entropy loss. The CSP, in fact, works well when there are a lot of data for each subject and this isn't the case. The small amount of data for the calibration of the BMI is a common problem in BMI applications [80], especially for the BMI used is clinical environment. This fact must be taken into account in the development of a BMI protocol. So considering the case without CSP, the LDA is the classifier that has the best performance on average, both in accuracy and in cross-entropy loss

(Table 4.4). This was also anticipated by Table 4.3 where is possible to see that in the case without CSP the bigger values of mean accuracy (in bold) are mixed between the three classifiers, while the smaller 'min c.e loss' belong 5 times at the LDA classificator and the smaller values of 'mean c.e loss' belong 4 times to LDA case. This provides that the LDA will be the classifier with the best performance. Starting from this, for the computing of the smoothing factor I used the predicted probabilities computed on the validation set with the small cross entropy loss. In Table 4.5 there is the smoothing factor chosen for each subject, so that gave a bigger area under the ROC curve. In Figure 4.6 I considered the case of a mean subject and analyze the accumulation probabilities for the two classes. Is shown as the mean value for pre-movement (Figure 4.6b) stays over the default probability threshold of 0.5, this implies that our classifier on average classifies correctly the pre-movement trial. But the probabilities still stand under 0.6, while I hope probabilities that increase more. Furthermore at the start of the pre-movement trial the standard deviation (SD) stays under the 0.5 value, this implies that in some cases, the pre-movement trial is initialy confused with a fixation trial. For the fixation case (Figure 4.6a) the average behavior stays under the 0.5 value, so in general the fixation trial is correctly classified, in fact in this case also the SD never overcome the 0.5 value. Notice that the SD go under the 0.4 values, so it means that for some subject the fixation trial is classified very well. Once the threshold was selectioned I was also interested in the comparison between the number of true positive and that of false positive (Table 4.6). In fact I ideally want that all the pre-movement trials are correctly classified, so the number of TP correspond to that of the pre-movement trials, and then all the fixation trials are correctly classified, so the number of FP is zero. The best result is obtained by S.05 with a

75% TPR of the pre-movement trials and a none of the fixation trials are missclassified. Similarly, S.01 achieved a good movement prediction while generating only a few false positive commands. The worst cases are the S.02 and the S.07. S.02 shows TPR and FPR performance close to the chance level, while S.07 shows a bias towards the positive class as he presents both a high TPR and FPR. Noticed that all the best thresholds are in the range 0.5-0.65. In fact in Figure 4.7 and from 7.13 to 7.18 is possibile to see how, with the value of α that is fixed, the TPR and FPR trend change with the change of the threshold value. The changing in the TP/FP rate is localized in the 0.4-0.7 range, while before 0.4 there is the 100% of TPR and FPR and after 0.7 there is small value of TPR and 0% of FPR.

5.1 Limitation

This work presents some limitations that should be accounted for in future work. The first limition was the small dataset collected for each subject. As shown by recent literature on BMI [81, 82, 83], to obtain stable features and high classification performance it is important to create a mutual interaction between the user and the BMI decoder. However, this can be achieved after several sessions of BMI training, as shown in [84, 85]. On the other hand, in this work I could analyse only the performances in a single session due to time limitations, preventing any user learning effect that could have improved the classification performance. Furthermore for the subjects S.04 and S.05 I couldn't record 5 runs due to technical problems during the experiments. In future, a longitudinal training of the BMI in a closed-loop conditions should be considered to overcome this limitation. In this experiment I try to make the protocol more realistic and like to a real 'everyday' situation. This

brings to some results that are logically less evident respect to a 'laboratory case'. For example the use of the walker to maintain the balance can divert the subject's attention from the movement of the lower limb to that of the hands, also activating some parts of the cortex that aren't connected to a lower limb motor execution. Furthermore the possible loss of balance can bring to a muscular artifact. This muscular artifact is a bit deleted by the laplacian filter but surely remains alterating our EEG dataset. A possible solution to this problem could be increase the time of the 'familiarization' session to make the subject more confident with the equipment and use other real time filters to a better cancellation of the muscular artifact. For example a Indipendent Component Analysis can be a solution, but it is a non-real time filter, so it is necessary to take it and find a real time application.

6 | Conclusions

In this thesis I propose and implemented a calibration protocol for a BMI-driven robotic exoskeleton. The peculiarity of this protocol was the idea of detecting a self-paced movement intention of the subject. The exoskeleton has been programmed to follow it and thanks to ROS architecture the three computer needed for the sight of the protocol, the movement of the exoskeleton and the acquisition of the EEG signal were connected. The computing of PSD was at the base for the detection of the pre-movement state of the person. Three classifiers were used to this purpose and the LDA is shown to be the more accurate. To increase the classification robustness, an exoponential integator was used to enhance the results. The final BMI system obtained an average prediction accuracy of lower limb movement of 76.32% with a false positive rate of 31.46%. Even if this performance must be improved to be effectively used as controlled input of the exoskeleton, the obtained results within a single-session recording are promising and comparable with BMI performance in the literature. In fact, I believe that the use of this BMI paradigm in a long-term training protocol will significantly improve the performance, following the concept of mutual learning between the user and the interface.

7 | Additional files

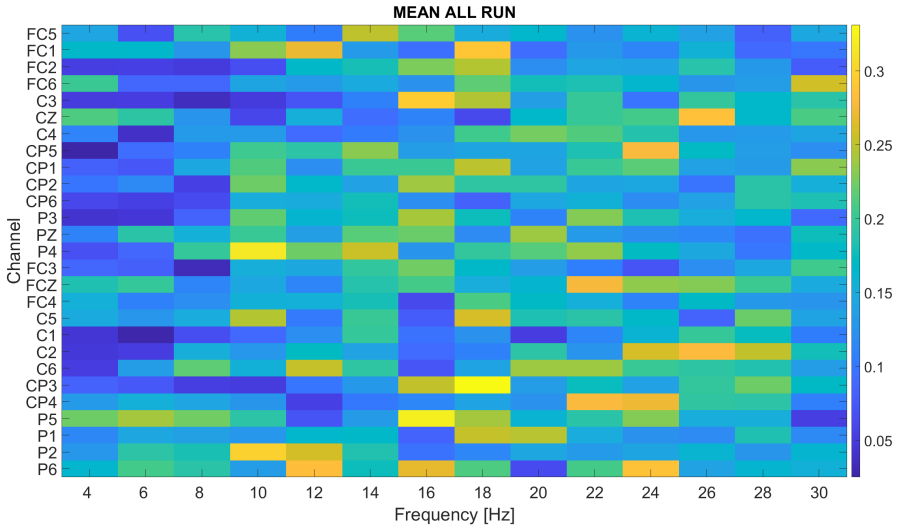

(a)

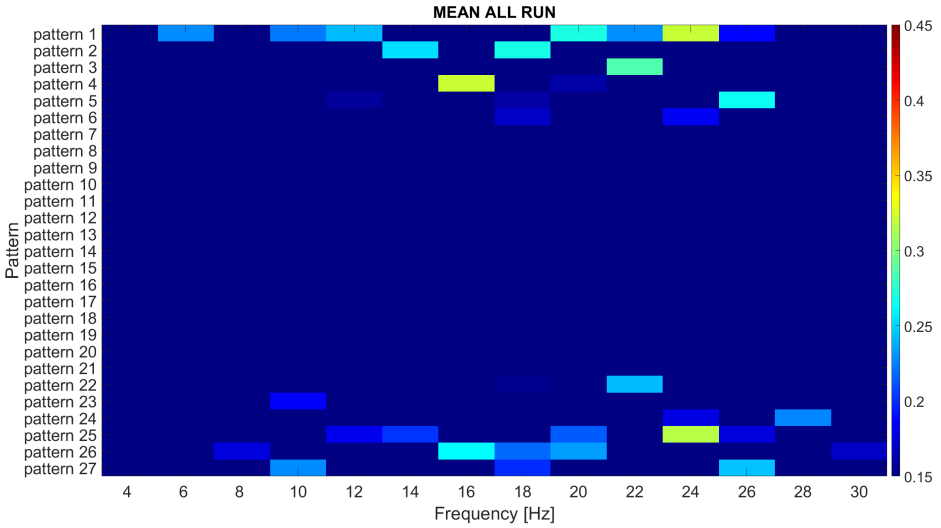

(b)

Figure 7.1: Features map S.02 (a), Features map CSP S.02 (b)

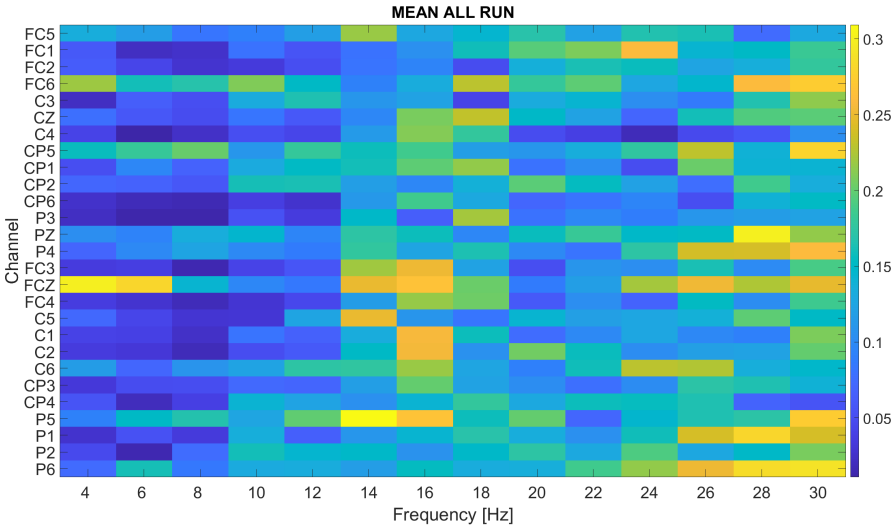

(a)

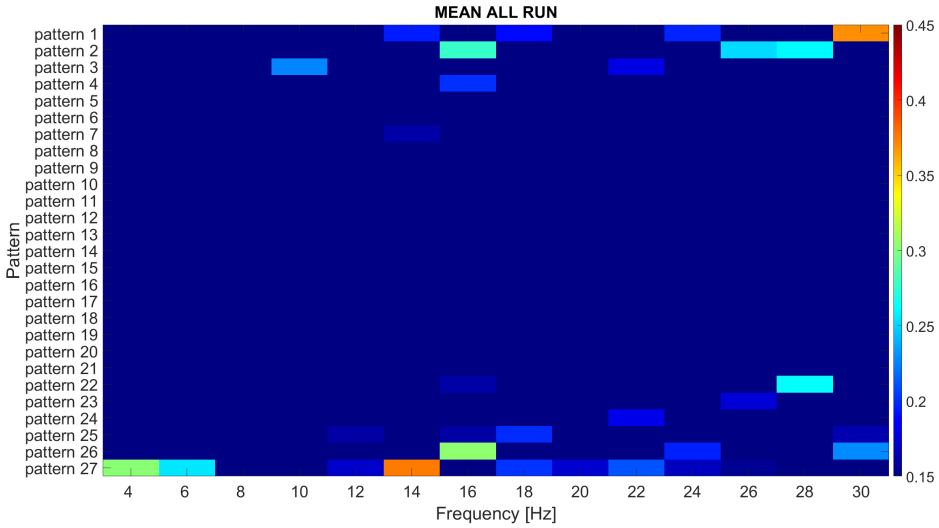

(b)

Figure 7.2: Features map S.03 (a), Features map CSP S.03 (b)

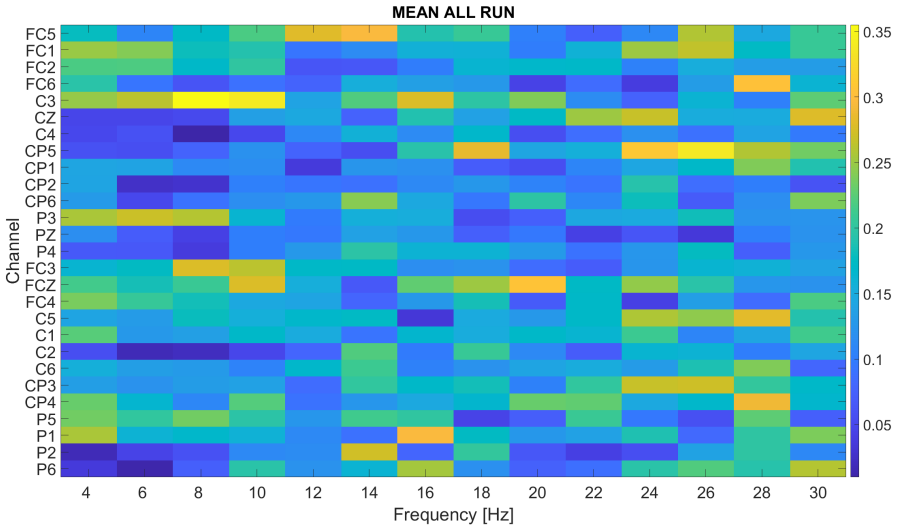

(a)

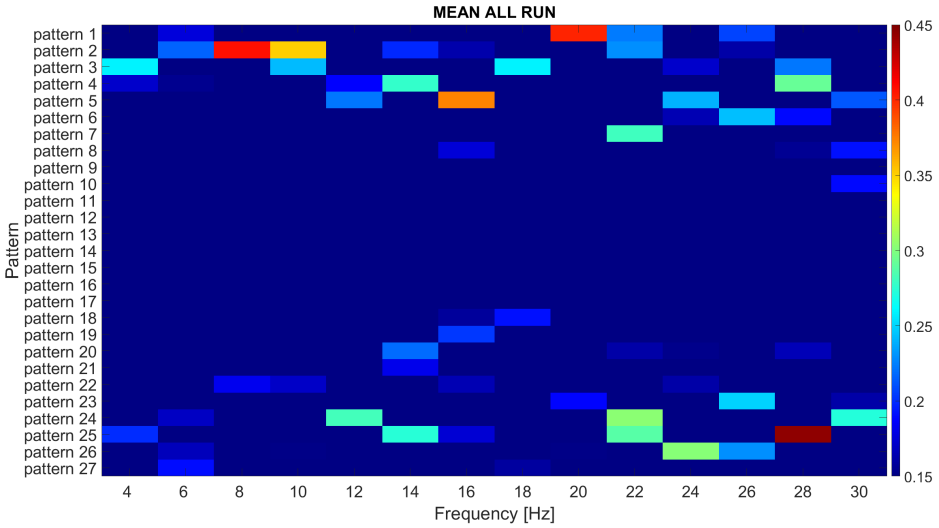

(b)

Figure 7.3: Features map S.04 (a), Features map CSP S.04 (b)

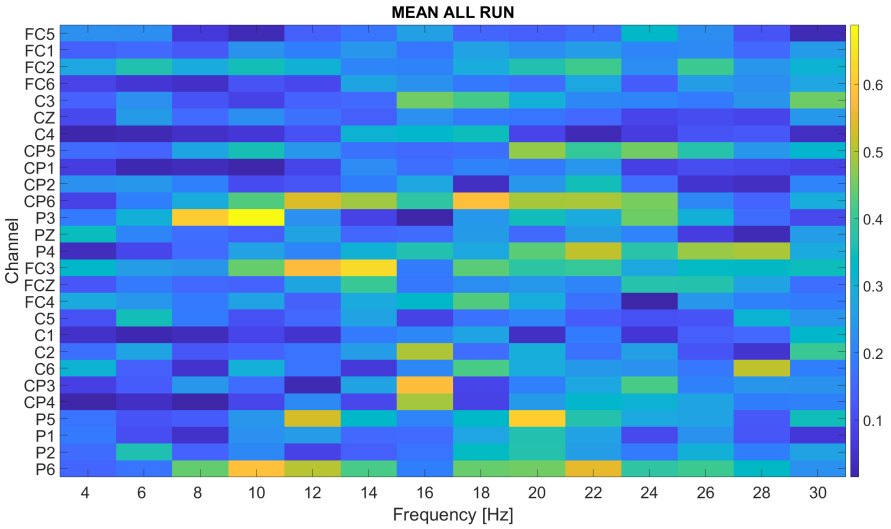

(a)

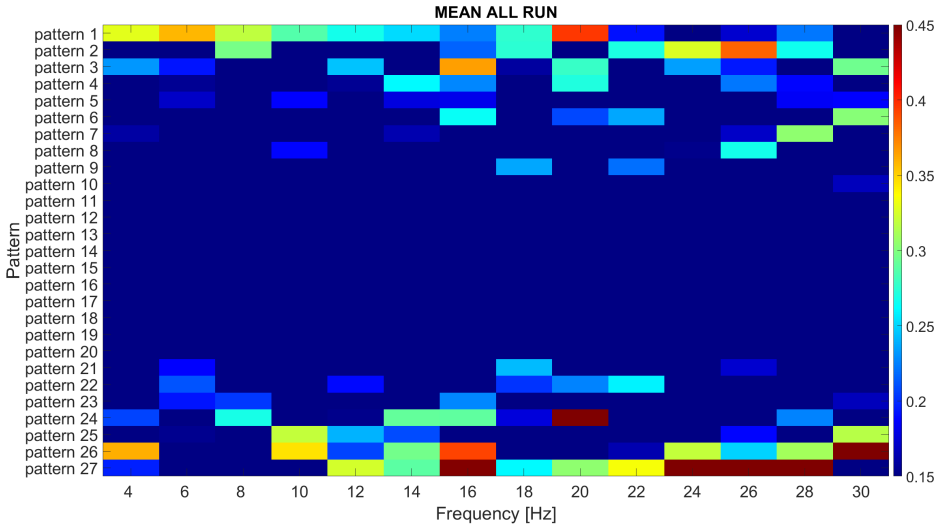

(b)

Figure 7.4: Features map S.05 (a), Features map CSP S.05 (b)

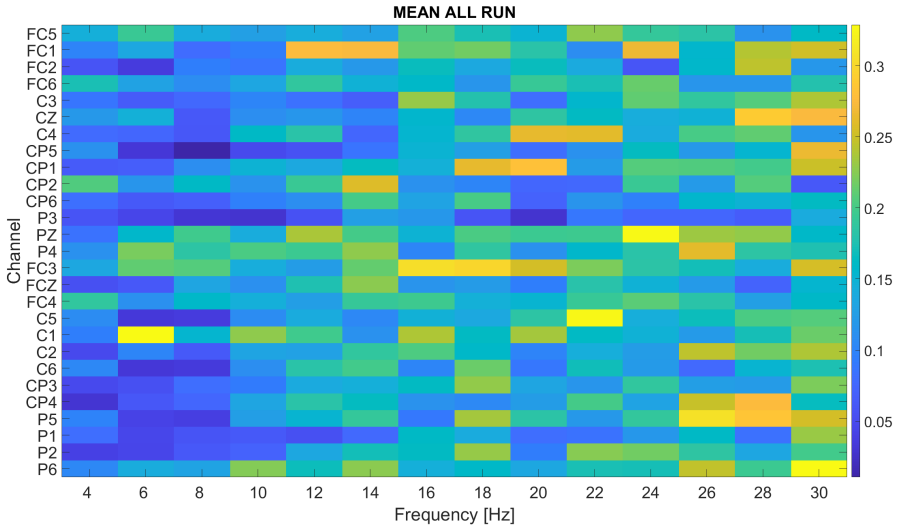

(a)

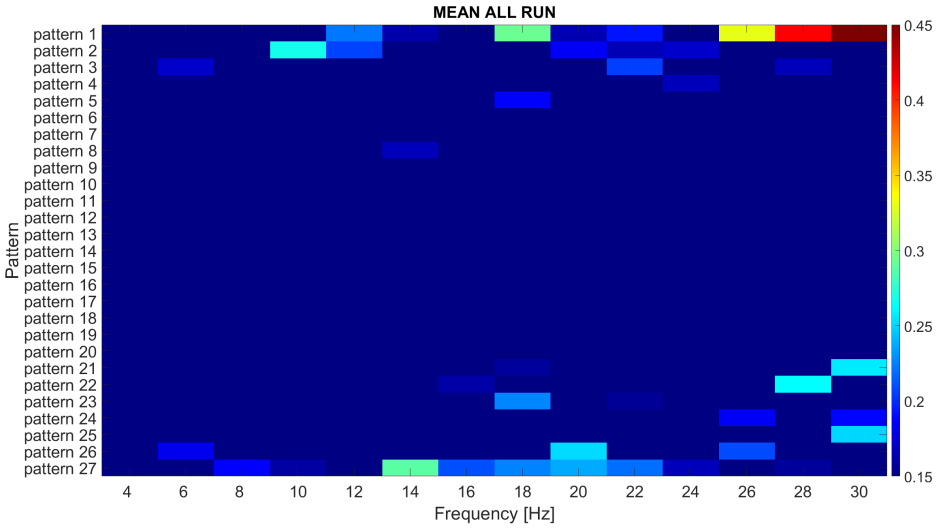

(b)

Figure 7.5: Features map S.06 (a), Features map CSP S.06 (b)

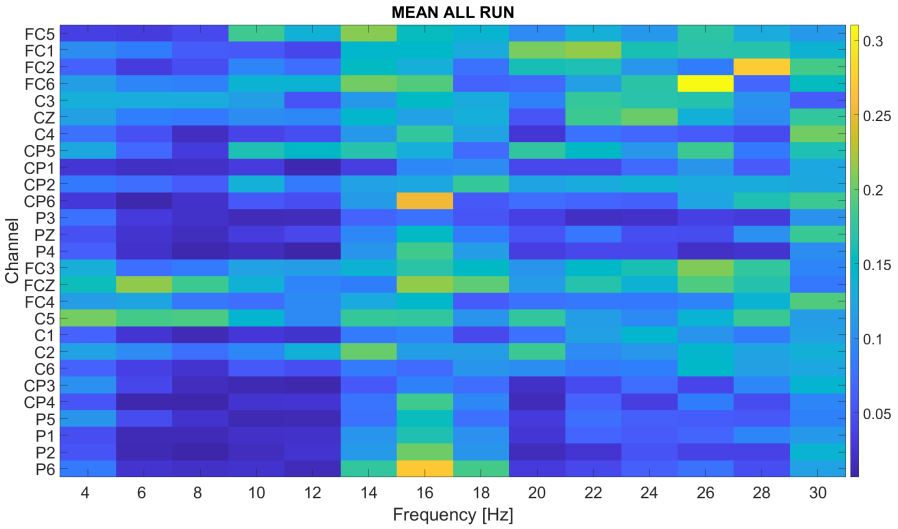

(a)

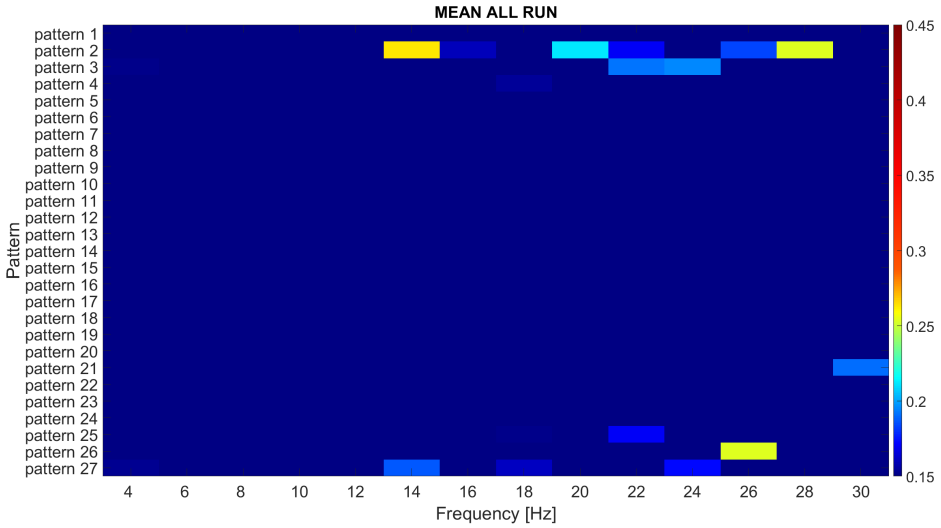

(b)

Figure 7.6: Features map S.07 (a), Features map CSP S.07 (b)

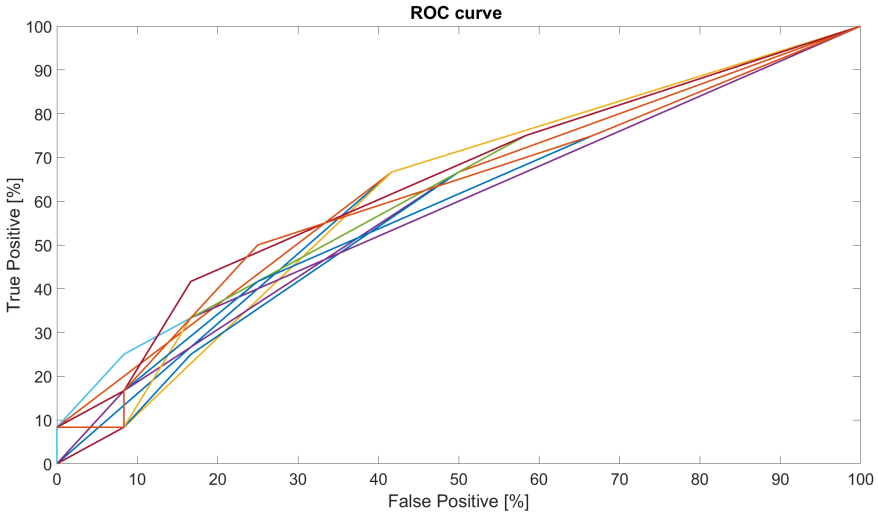

(a)

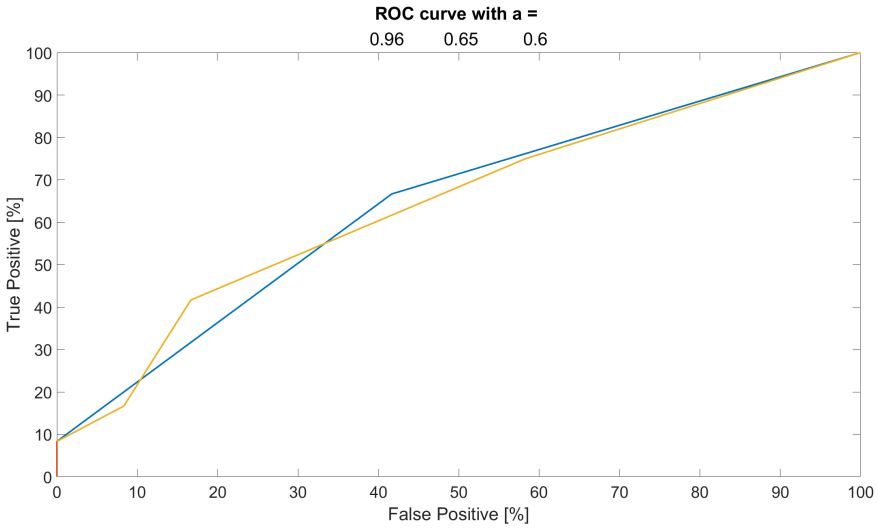

(b)

Figure 7.7: ROC curves for S.02 (a), ROC curve with the best AUC for S.02 (b)

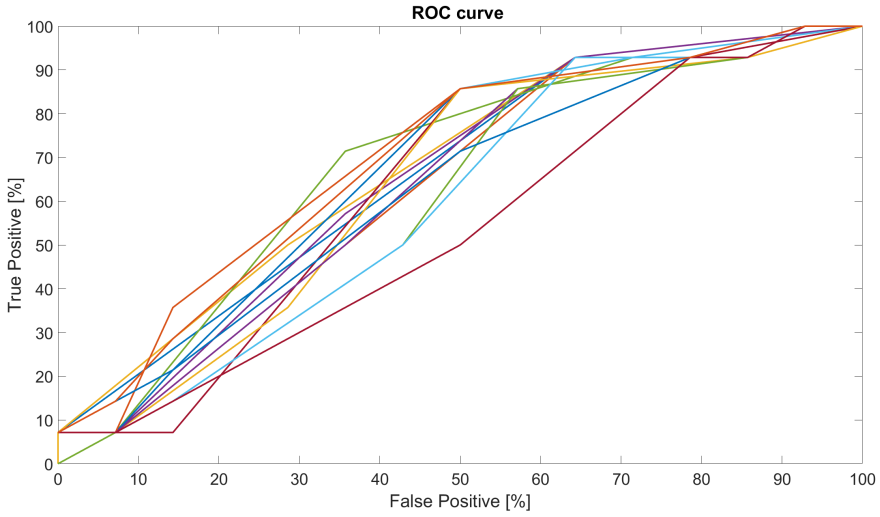

(a)

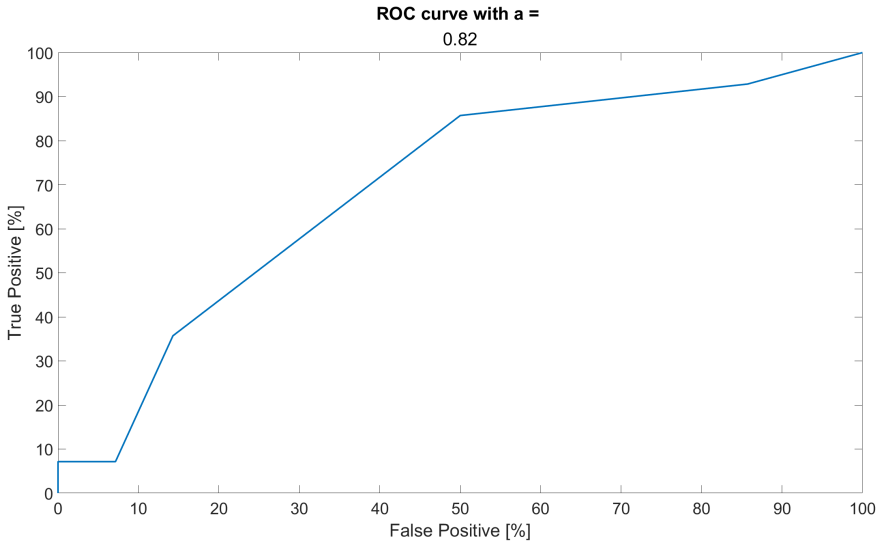

(b)

Figure 7.8: ROC curves for S.03 (a), ROC curve with the best AUC for S.03 (b)

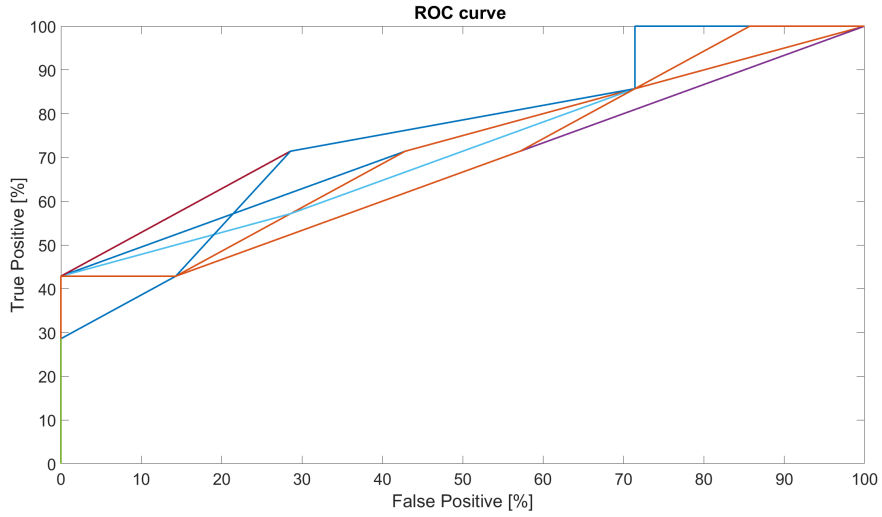

(a)

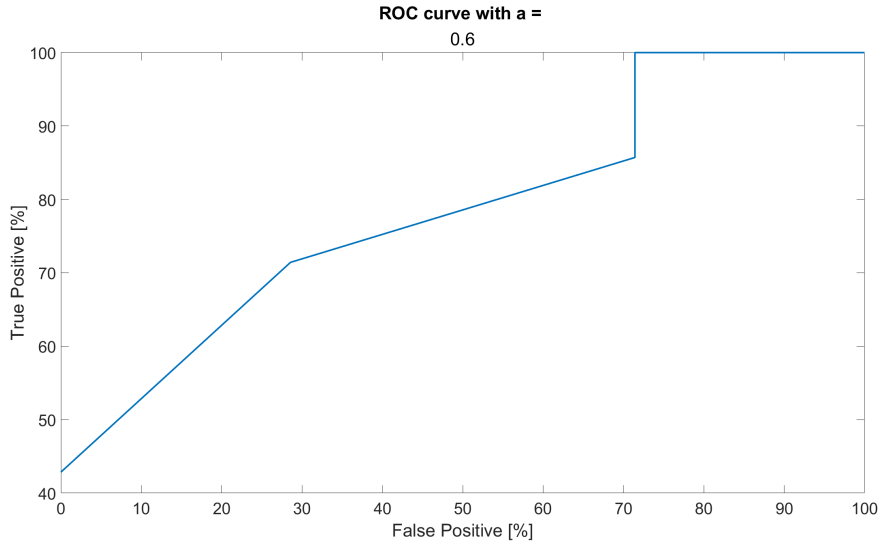

(b)

Figure 7.9: ROC curves for S.04 (a), ROC curve with the best AUC for S.04 (b)

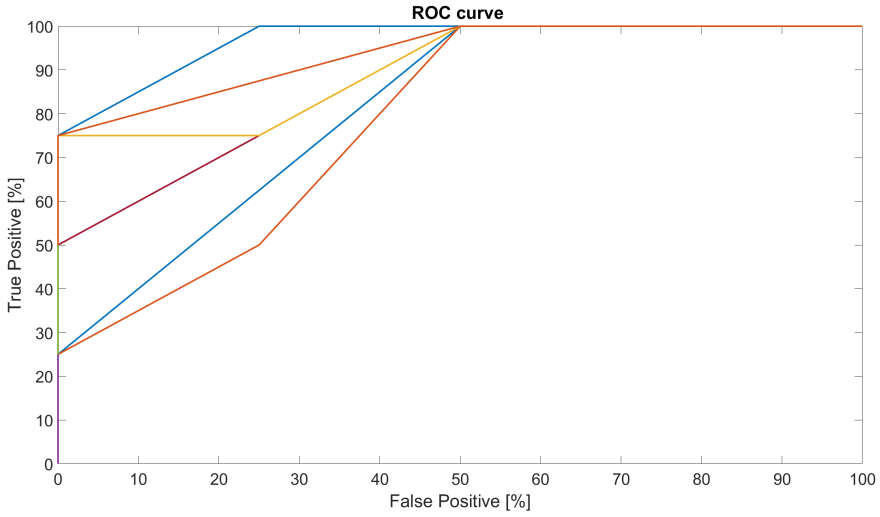

(a)

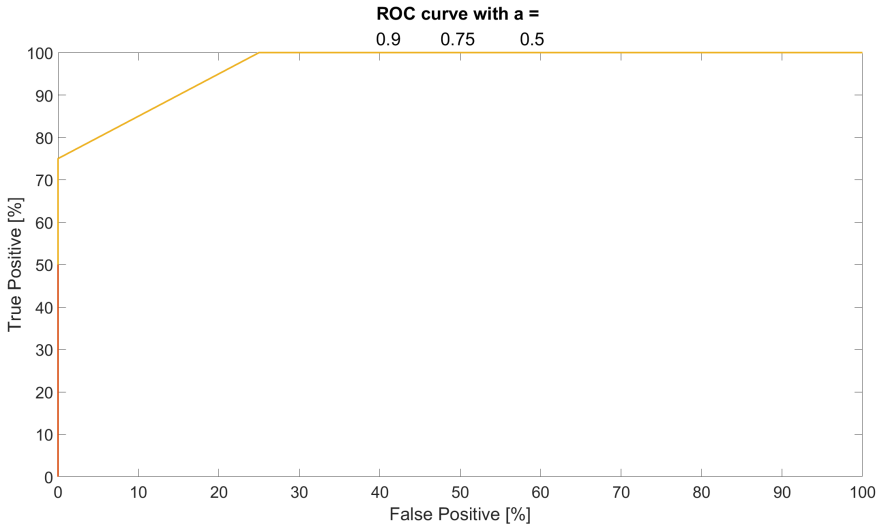

(b)

Figure 7.10: ROC curves for S.05 (a), ROC curve with the best AUC for S.05 (b)

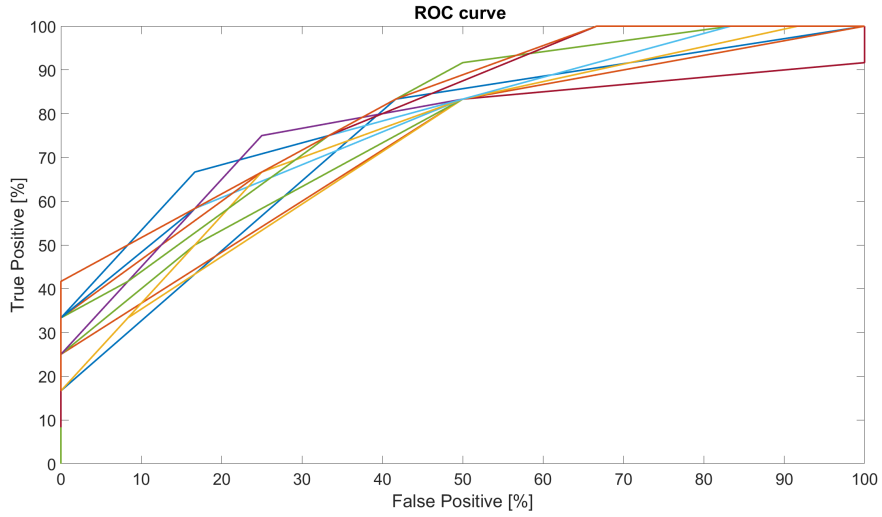

(a)

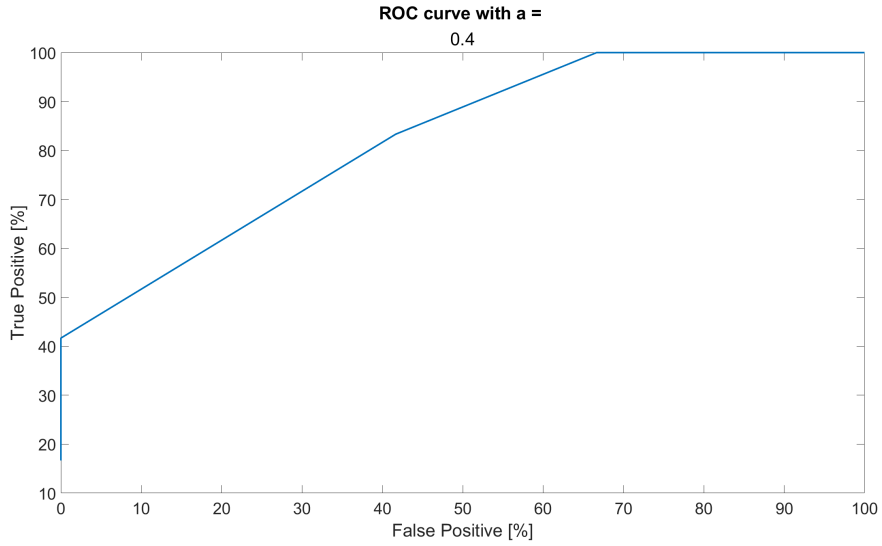

(b)

Figure 7.11: ROC curves for S.06 (a), ROC curve with the best AUC for S.06 (b)

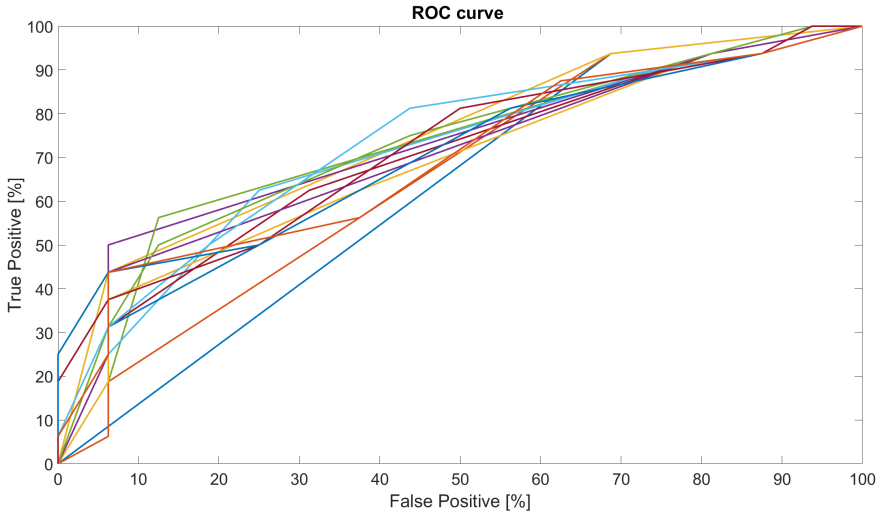

(a)

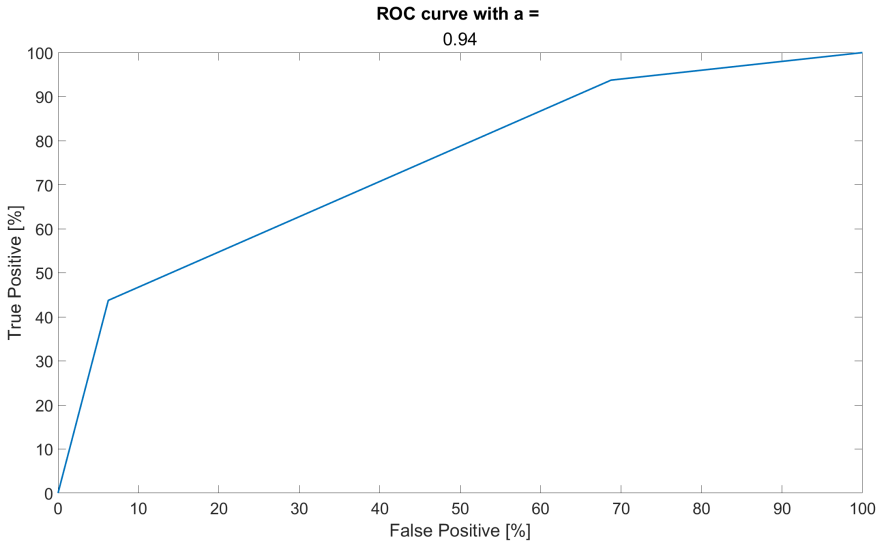

(b)

Figure 7.12: ROC curves for S.07 (a), ROC curve with the best AUC for S.07 (b)

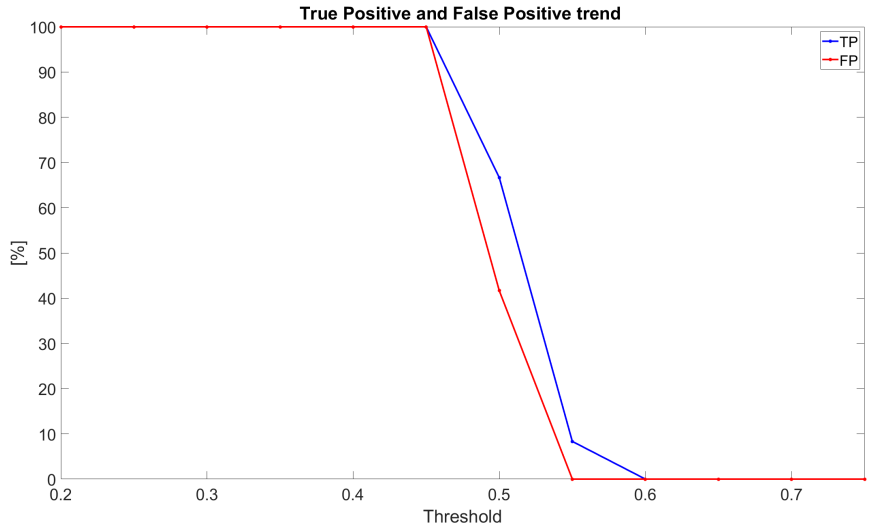

Figure 7.13: Trend of TPR and FPR of S.02

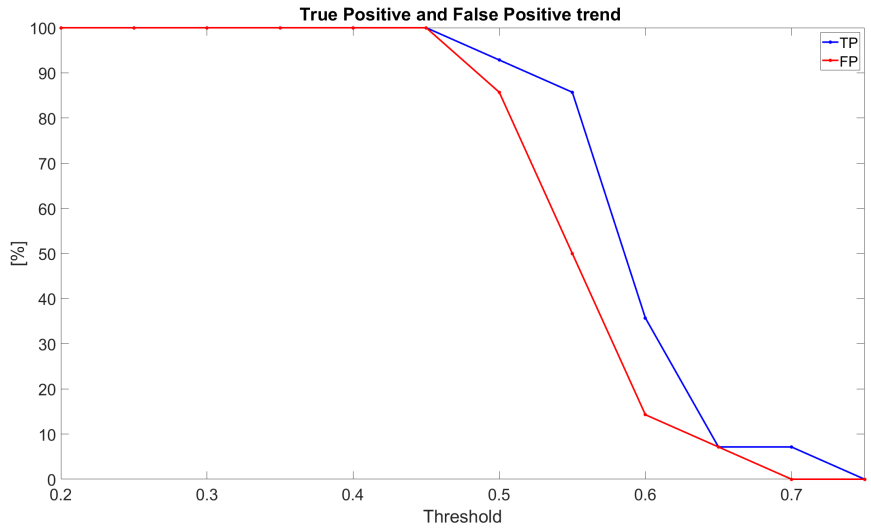

Figure 7.14: Trend of TPR and FPR of S.03

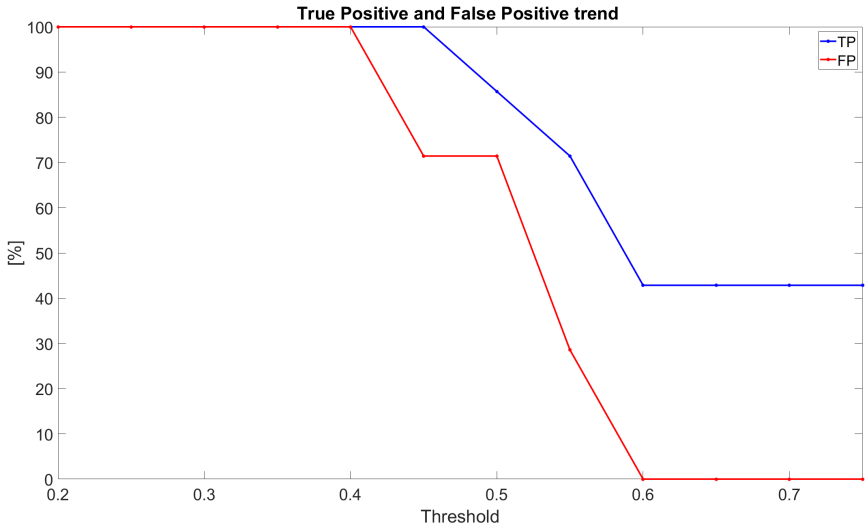

Figure 7.15: Trend of TPR and FPR of S.04

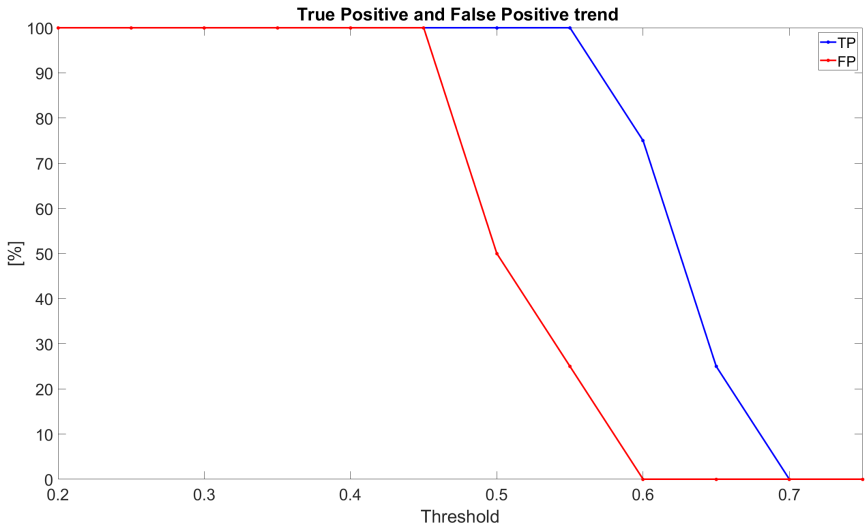

Figure 7.16: Trend of TPR and FPR of S.05

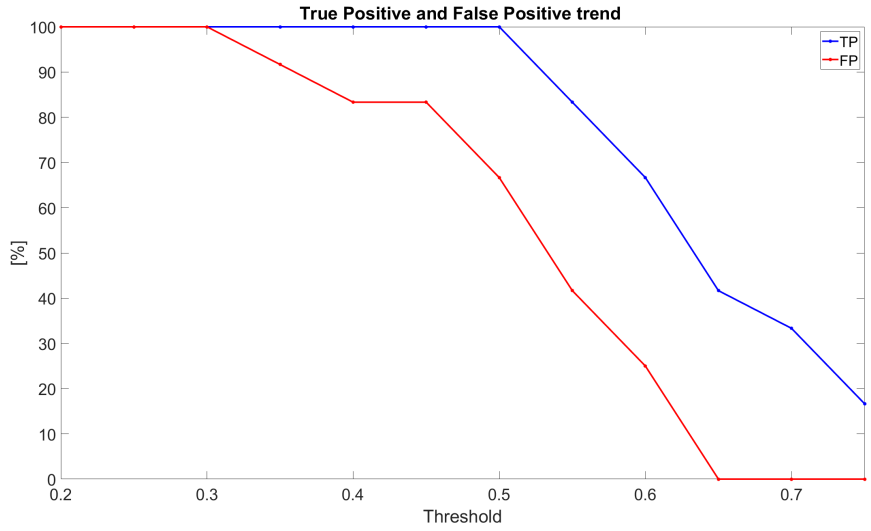

Figure 7.17: Trend of TPR and FPR of S.06

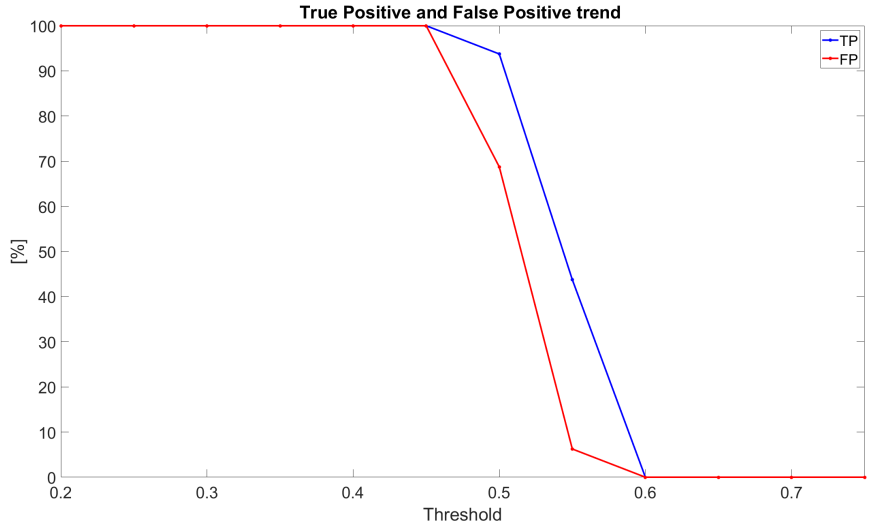

Figure 7.18: Trend of TPR and FPR of S.07

Bibliography

[1] *Oxford English Dictionary, The Definitive Record of the English Language*. 2022.

[2] C. A.A., "Western Medical Rehabilitation through Time: A Historical and Epistemological Review," *ScientificWorldJournal*, 2014.

[3] A. Pollock, G. Baer, P. Langhorne, and V. Pomeroy, "Physiotherapy treatment approaches for the recovery of postural control and lower limb function following stroke: a systematic review," *Clinical Rehabilitation*, vol. 21, no. 5, pp. 395–410, 2007. PMID: 17613560.

[4] R. H. Benedict, R. Holtzer, R. W. Motl, F. W. Foley, S. Kaur, D. Hojnacki, and B. Weinstock-Guttman, "Upper and lower extremity motor function and cognitive impairment in multiple sclerosis," *Journal of the International Neuropsychological Society*, vol. 17, no. 4, p. 643–653, 2011.

[5] H. Cianci, "Falling in parkinson disease: identifying and prioritizing risk factors in recurrent fallers. dennison ac, noorigian jv, robinson km, fisman dn, cianci hj, moberg p, bunting-perry l, martine r, duda j, stern mb. am j phys med rehabil. 2007 aug;86(8):621-32.," 01 2007.

[6] P. Freund, N. Weiskopf, N. S. Ward, C. Hutton, A. Gall, O. Ciccarelli, M. Craggs, K. Friston, and A. J. Thompson, "Disability, atrophy and cortical reorganization following spinal cord injury," *Brain*, vol. 134, pp. 1610–1622, 05 2011.

[7] T. Castermans, M. Duvinage, G. Cheron, and T. Dutoit, "Towards effective non-invasive brain-computer interfaces dedicated to gait rehabilitation systems," *Brain Sciences*, vol. 4, pp. 1–48, 03 2013.

[8] M. Kyrarini, F. Lygerakis, A. Rajavenkatanarayanan, C. Sevastopoulos, H. R. Nambiappan, K. K. Chaitanya, A. R. Babu, J. Mathew, and F. Makedon, "A survey of robots in healthcare," *Technologies*, vol. 9, no. 1, 2021.

[9] H. Lee, P. W. Ferguson, and J. Rosen, "Chapter 11 - lower limb exoskeleton systems—overview," in *Wearable Robotics* (J. Rosen and P. W. Ferguson, eds.), pp. 207–229, Academic Press, 2020.

[10] M. Goffredo, C. Iacovelli, E. Russo, S. Pournajaf, C. Di Blasi, D. Galafate, L. Pellicciari, M. Agosti, S. Filoni, I. Aprile, and M. Franceschini, "Stroke gait rehabilitation: A comparison of end-effector, overground exoskeleton, and conventional gait training," *Applied Sciences*, vol. 9, no. 13, 2019.

[11] R. Nudo, G. Milliken, W. Jenkins, and M. Merzenich, "Use-dependent alterations of movement representations in primary motor cortex of adult squirrel monkeys," *Journal of Neuroscience*, vol. 16, no. 2, pp. 785–807, 1996.

[12] C. Wang, X. Wu, Z. Wang, and Y. Ma, "Implementation of a brain-computer interface on a lower-limb exoskeleton," *IEEE Access*, vol. 6, pp. 38524–38534, 2018.

[13] M. Iosa, G. Morone, A. Cherubini, and P. S., "The three laws of neurorobotics: A review on what neurorehabilitation robots should do for patients and clinicians," *J Med Biol Eng.*, vol. 36, pp. 1–11, 2016.

[14] E. López-Larraz, F. Trincado-Alonso, V. Rajasekaran, S. Pérez-Nombela, A. J. del Ama, J. Aranda, J. Minguez, A. Gil-Agudo, and L. Montesano, "Control of an ambulatory exoskeleton with a brain–machine interface for spinal cord injury gait rehabilitation," *Frontiers in Neuroscience*, vol. 10, 2016.

[15] F. H. McDOWELL, *Neurorehabilitation.* 1994.

[16] T. Renton, A. Tibbles, and J. Topolovec-Vranic, "Neurofeedback as a form of cognitive rehabilitation therapy following stroke: A systematic review," *Archives of Physical Medicine and Rehabilitation*, vol. 96, p. e27, 12 2015.

[17] O. R. Dobrushina, R. M. Vlasova, A. D. Rumshiskaya, L. D. Litvinova, E. A. Mershina, V. E. Sinitsyn, and E. V. Pechenkova, "Modulation of intrinsic brain connectivity by implicit electroencephalographic neurofeedback," *Frontiers in Human Neuroscience*, vol. 14, 2020.

[18] W. Alvarado-Díaz, P. Lima, B. Meneses-Claudio, and A. Roman-Gonzalez, "Implementation of a brain-machine interface for controlling a wheelchair," in *2017 CHILEAN Conference on Electrical, Electronics Engineering, Information and Communication Technologies (CHILECON)*, pp. 1–6, 2017.

[19] M. S. Fifer, S. Acharya, H. L. Benz, M. Mollazadeh, N. E. Crone, and N. V. Thakor, "Toward electrocorticographic control of a dexterous upper limb prosthesis: Building brain-machine interfaces," *IEEE Pulse*, vol. 3, no. 1, pp. 38–42, 2012.

[20] A. H. Do, P. T. Wang, C. E. King, S. N. Chun, and Z. Nenadic, "Brain-computer interface controlled robotic gait orthosis," 2012.

[21] J. Wolpaw, N. Birbaumer, W. Heetderks, D. Mcfarland, P. Peckham, G. Schalk, E. Donchin, L. Quatrano, C. Robinson, and T. Vaughan, "Brain-computer interface technology: A review of the first international meeting," *IEEE transactions on rehabilitation engineering : a publication of the IEEE Engineering in Medicine and Biology Society*, vol. 8, pp. 164–73, 07 2000.

[22] J. d. R. Millán, R. Rupp, G. Mueller-Putz, R. Murray-Smith, C. Giugliemma, M. Tangermann, C. Vidaurre, F. Cincotti, A. Kubler, R. Leeb, C. Neuper, K. Mueller, and D. Mattia, "Combining brain–computer interfaces and assistive technologies: State-of-the-art and challenges," *Frontiers in Neuroscience*, vol. 4, 2010.

[23] U. Chaudhary, N. Birbaumer, and A. Ramos-Murguialday, "Brain–computer interfaces for communication and rehabilitation," *Nature Reviews Neurology*, vol. 12, pp. 513–525, 2016.

[24] S. Perdikis and J. d. R. Millan, "Brain-machine interfaces: A tale of two learners," *IEEE Systems, Man, and Cybernetics Magazine*, vol. 6, no. 3, pp. 12–19, 2020.

[25] J. Ahmed, "Brain machine interface using eeg sci-fi to reality neural interface engineering brain machine interface using eeg 1 brain machine interface using eeg," 12 2016.

[26] A. Shah and S. Mittal, "Invasive electroencephalography monitoring: Indications and presurgical planning," *Annals of Indian Academy of Neurology*, vol. 17, pp. S89–S94, 03 2014.

[27] L. Tonin and J. d. R. Millán, "Noninvasive brain–machine interfaces for robotic devices," *Annual Review of Control, Robotics, and Autonomous Systems*, vol. 4, no. 1, pp. 191–214, 2021.

[28] D. Heeger and D. Ress, "What does fmri tell us about neuronal activity?," *Nature reviews. Neuroscience*, vol. 3, pp. 142–51, 03 2002.

[29] P. Pinti, I. Tachtsidis, A. Hamilton, J. Hirsch, C. Aichelburg, S. Gilbert, and P. W. Burgess, "The present and future use of functional near-infrared spectroscopy (fnirs) for cognitive neuroscience," *Annals of the New York Academy of Sciences*, vol. 1464, no. 1, pp. 5–29, 2020.

[30] M. Rea, N. Holmes, R. M. Hill, E. Boto, J. Leggett, L. J. Edwards, D. Woolger, E. Dawson, V. Shah, J. Osborne, R. Bowtell, and M. J. Brookes, "Precision magnetic field modelling and control for wearable magnetoencephalography," *NeuroImage*, vol. 241, p. 118401, 2021.

[31] Y. F. Tai and P. Piccini, "Applications of positron emission tomography (pet) in neurology," *Journal of Neurology, Neurosurgery & Psychiatry*, vol. 75, no. 5, pp. 669–676, 2004.

[32] N. Xu, W. Shan, J. Qi, J. Wu, and Q. Wang, "Presurgical evaluation of epilepsy using resting-state meg functional connectivity," *Frontiers in Human Neuroscience*, vol. 15, 2021.

[33] M. Soufineyestani, D. Dowling, and A. Khan, "Electroencephalography (eeg) technology applications and available devices," *Applied Sciences*, vol. 10, no. 21, 2020.

[34] R. Gupta and T. H. Falk, "Affective state characterization based on electroencephalography graph-theoretic features," in *2015 7th International IEEE/EMBS Conference on Neural Engineering (NER)*, pp. 577–580, 2015.

[35] P. Cardellicchio, P. M. Hilt, E. Dolfini, L. Fadiga, and A. D'Ausilio, "Beta rebound as an index of temporal integration of somatosensory and motor signals," *Frontiers in Systems Neuroscience*, vol. 14, 2020.

[36] M. Schreuder, J. Höhne, B. Blankertz, S. Haufe, T. Dickhaus, and M. Tangermann, "Optimizing event-related potential based brain-computer interfaces: A systematic evaluation of dynamic stopping methods," *Journal of neural engineering*, vol. 10, p. 036025, 05 2013.

[37] E. B. Coffey, A.-M. Brouwer, E. S. Wilschut, and J. B. van Erp, "Brain–machine interfaces in space: Using spontaneous rather than intentionally generated brain signals," *Acta Astronautica*, vol. 67, no. 1, pp. 1–11, 2010.

[38] S. Sur and V. K. Sinha, "Event-related potential: An overview," *Industrial Psychiatry Journal*, vol. 18, pp. 70 – 73, 2009.

[39] A. M. Norcia, L. G. Appelbaum, J. M. Ales, B. R. Cottereau, and B. Rossion, "The steady-state visual evoked potential in vision research: A review," *Journal of Vision*, vol. 15, pp. 4–4, 05 2015.

[40] D. E. J. Linden, "The p300: Where in the brain is it produced and what does it tell us?," *The Neuroscientist*, vol. 11, no. 6, pp. 563–576, 2005. PMID: 16282597.

[41] R. Chavarriaga, A. Sobolewski, and J. d. R. Millán, "Errare machinale est: the use of error-related potentials in brain-machine interfaces," *Frontiers in Neuroscience*, vol. 8, 2014.

[42] M. P. Branco, L. M. de Boer, N. F. Ramsey, and M. J. Vansteensel, "Encoding of kinetic and kinematic movement parameters in the sensorimotor cortex: A brain-computer interface perspective," *European Journal of Neuroscience*, vol. 50, no. 5, pp. 2755–2772, 2019.

[43] H. Yuan and B. He, "Brain-computer interfaces using sensorimotor rhythms: Current state and future perspectives," *IEEE transactions on bio-medical engineering*, vol. 61, pp. 1425–35, 05 2014.

[44] R. Bauer, M. Fels, M. Vukelić, U. Ziemann, and A. Gharabaghi, "Bridging the gap between motor imagery and motor execution with a brain–robot interface," *NeuroImage*, vol. 108, pp. 319–327, 2015.

[45] R. Lubbe, J. Sobierajewicz, M. Jongsma, W. Verwey, and A. Przekoracka-Krawczyk, "Frontal brain areas are more involved during motor imagery than during motor execution/preparation of a response sequence," *International Journal of Psychophysiology*, vol. 164, 02 2021.

[46] A. Kübler and D. Mattia, "Chapter 14 - brain–computer interface based solutions for end-users with severe communication disorders," in *The Neurology of Conciousness (Second Edition)* (S. Laureys, O. Gosseries, and G. Tononi, eds.), pp. 217–240, San Diego: Academic Press, second edition ed., 2016.

[47] B. He, B. Baxter, B. J. Edelman, C. C. Cline, and W. W. Ye, "Noninvasive brain-computer interfaces based on sensorimotor rhythms," *Proceedings of the IEEE*, vol. 103, no. 6, pp. 907–925, 2015.

[48] G. Pfurtscheller, "Event-related eeg/meg synchronization and desynchronization: basic principles.," *Clinical neurophysiology.*, vol. 110, no. 11, 1999-10-31.

[49] K. J. Miller, G. Schalk, E. E. Fetz, M. den Nijs, J. G. Ojemann, and R. P. N. Rao, "Cortical activity during motor execution, motor imagery, and imagery-based online feedback," *Proceedings of the National Academy of Sciences*, vol. 107, no. 9, pp. 4430–4435, 2010.

[50] G. Pfurtscheller and C. Neuper, "Motor imagery activates primary sensorimotor area in humans," *Neuroscience Letters*, vol. 239, no. 2, pp. 65–68, 1997.

[51] S. Rimbert, L. Bougrain, C. Lindig, and G. Serrière, "Modulation of beta power in eeg during discrete and continuous motor imageries," 04 2015.

[52] A. N. Belkacem, N. Jamil, J. A. Palmer, S. Ouhbi, and C. Chen, "Brain computer interfaces for improving the quality of life of older adults and elderly patients," *Frontiers in Neuroscience*, vol. 14, 2020.

[53] V. Asanza, C. Pelaez, F. Loayza, L. Lorente, and D. Peluffo, "Identification of lower-limb motor tasks via brain–computer interfaces: A topical overview," *Sensors*, vol. 22, p. 2028, 03 2022.

[54] D. Liu, W. Chen, K. Lee, Z. Pei, and J. d. R. Millán, "An eeg-based brain-computer interface for gait training," *2017 29th Chinese Control And Decision Conference (CCDC)*, pp. 6755–6760, 2017.

[55] L. Ferrero, V. Quiles, M. Ortiz, E. Iáñez, and J. M. Azorín, "A bmi based on motor imagery and attention for commanding a lower-limb robotic exoskeleton: A case study," *Applied Sciences*, vol. 11, no. 9, 2021.

[56] Z. Wang, C. Wang, G. Wu, Y. Luo, and X. Wu, "A control system of lower limb exoskeleton robots based on motor imagery," in *2017 IEEE International Conference on Information and Automation (ICIA)*, pp. 311–316, 2017.

[57] J. Choi, K. T. Kim, J. H. Jeong, L. Kim, S. J. Lee, and H. Kim, "Developing a motor imagery-based real-time asynchronous hybrid bci controller for a lower-limb exoskeleton," *Sensors*, vol. 20, no. 24, 2020.

[58] A.-I. Sburlea, L. Montesano, R. Cano de la Cuerda, I. Alguacil, j.-c. Page, and J. Minguez, "Detecting intention to walk in stroke patients from pre-movement eeg correlates," *Journal of NeuroEngineering and Rehabilitation*, vol. 12, 12 2015.

[59] A.-I. Sburlea, L. Montesano, and J. Minguez, "Continuous detection of the self-initiated walking pre-movement state from eeg correlates without session-to-session recalibration," *Journal of neural engineering*, vol. 12, p. 036007, 04 2015.

[60] D. Liu, W. Chen, K. Lee, R. Chavarriaga, F. Iwane, M. Bouri, Z. Pei, and J. d. R. Millán, "Eeg-based lower-limb movement onset decoding: Continuous classification and asynchronous detection," *IEEE Transactions on Neural Systems and Rehabilitation Engineering*, vol. 26, no. 8, pp. 1626–1635, 2018.

[61] C. Wang, X. Wu, Z. Wang, and Y. Ma, "Implementation of a brain-computer interface on a lower-limb exoskeleton," *IEEE Access*, vol. 6, pp. 38524–38534, 2018.

[62] M. Cardona, C. E. García Cena, F. Serrano, and R. Saltaren, "Alice: Conceptual development of a lower limb exoskeleton robot driven by an on-board musculoskeletal simulator," *Sensors*, vol. 20, no. 3, 2020.

[63] M. Cardona, "Kinematics solution of alice: An exoskeleton robot for rehabilitation," pp. 1–6, 2021.

[64] L. Tonin, G. Beraldo, S. Tortora, and E. Menegatti, "Ros-neuro: An open-source platform for neurorobotics," *Frontiers in Neurorobotics*, vol. 16, 2022.

[65] R. Behroozmand and S. Sangtian, "Neural bases of sensorimotor adaptation in the vocal motor system," *Experimental Brain Research*, vol. 236, 07 2018.

[66] D. J. McFarland, L. M. McCane, S. V. David, and J. R. Wolpaw, "Spatial filter selection for eeg-based communication," *Electroencephalography and Clinical Neurophysiology*, vol. 103, no. 3, pp. 386–394, 1997.

[67] S. Fitzgibbon, D. DeLosAngeles, T. Lewis, D. Powers, E. Whitham, J. Willoughby, and K. Pope, "Surface laplacian of scalp electrical signals and independent component analysis resolve emg contamination of electroencephalogram," *International Journal of Psychophysiology*, vol. 97, no. 3, pp. 277–284, 2015. On the benefits of using surface Laplacian (current source density) methodology in electrophysiology.

[68] O. M. Solomon, Jr, "Psd computations using welch's method. [power spectral density (psd)]," 12 1991.

[69] X. Song and S.-C. Yoon, "Improving brain-computer interface classification using adaptive common spatial patterns," *Computers in Biology and Medicine*, vol. 61, 03 2015.

[70] Wikipedia contributors, "Linear discriminant analysis — Wikipedia, the free encyclopedia," 2022. [Online; accessed 17-October-2022].

[71] Wikipedia contributors, "Bayes' theorem — Wikipedia, the free encyclopedia," 2022. [Online; accessed 18-October-2022].

[72] J. Tolles and W. J. Meurer, "Logistic Regression: Relating Patient Characteristics to Outcomes," *JAMA*, vol. 316, pp. 533–534, 08 2016.

[73] J. Ma and W. Gao, "The supervised learning gaussian mixture model," *J. Comput. Sci. Technol.*, vol. 13, pp. 471–474, 09 1998.

[74] S. Tortora, G. Beraldo, L. Tonin, and E. Menegatti, "Entropy-based motion intention identification for brain-computer interface," in *2019 IEEE International Conference on Systems, Man and Cybernetics (SMC)*, pp. 2791–2798, 2019.

[75] Wikipedia contributors, "Receiver operating characteristic — Wikipedia, the free encyclopedia," 2022. [Online; accessed 21-October-2022].

[76] G. Pfurtscheller and A. Aranibar, "Evaluation of event-related desynchronization (erd) preceding and following voluntary self-paced movement," *Electroencephalography and Clinical Neurophysiology*, vol. 46, no. 2, pp. 138–146, 1979.

[77] D. Liu, W. Chen, Z. Pei, and J. Wang, "Detection of lower-limb movement intention from eeg signals," pp. 84–89, 06 2017.

[78] J. Choi and H. Kim, "Real-time decoding of eeg gait intention for controlling a lower-limb exoskeleton system," in *2019 7th International Winter Conference on Brain-Computer Interface (BCI)*, pp. 1–3, 2019.

[79] G. Yu, J. Wang, W. Chen, and J. Zhang, "Eeg-based brain-controlled lower extremity exoskeleton rehabilitation robot," in *2017 IEEE International Conference on Cybernetics and Intelligent Systems (CIS) and IEEE Conference on Robotics, Automation and Mechatronics (RAM)*, pp. 763–767, 2017.

[80] D.-K. Han and J.-H. Jeong, "Domain generalization for session-independent brain-computer interface," in *2021 9th International Winter Conference on Brain-Computer Interface (BCI)*, pp. 1–5, 2021.

[81] L. Hehenberger, R. J. Kobler, C. Lopes-Dias, N. Srisrisawang, P. Tumfart, J. B. Uroko, P. R. Torke, and G. R. Müller-Putz, "Long-term mutual training for the cybathlon bci race with a tetraplegic pilot: A case study on inter-session transfer and intra-session adaptation," *Frontiers in Human Neuroscience*, vol. 15, 2021.

[82] A. Schwarz, D. Steyrl, and G. R. Müller-Putz, "Brain-computer interface adaptation for an end user to compete in the cybathlon," in *2016 IEEE International Conference on Systems, Man, and Cybernetics (SMC)*, pp. 001803–001808, 2016.

[83] D. J. McFarland and J. R. Wolpaw, "Brain–computer interface use is a skill that user and system acquire together," *PLOS Biology*, vol. 16, pp. 1–4, 07 2018.

[84] S. Perdikis, L. Tonin, S. Saeedi, C. Schneider, and J. d. R. Millán, "The cybathlon bci race: Successful longitudinal mutual learning with two tetraplegic users," *PLOS Biology*, vol. 16, pp. 1–28, 05 2018.

[85] S. Tortora, G. Beraldo, F. Bettella, E. Formaggio, M. Rubega, A. Del Felice, S. Masiero, R. Carli, N. Petrone, E. Menegatti, *et al.*, "Neural correlates of user learning during long-term bci training for the cybathlon competition," *Journal of NeuroEngineering and Rehabilitation*, vol. 19, no. 1, pp. 1–19, 2022.

[86] P. Di Nota, J. Chartrand, G. Levkov, R. Montefusco, and J. DeSouza, "Experience-dependent modulation of alpha and beta during action observation and motor imagery," *BMC Neuroscience*, vol. 18, 03 2017.

Acknowledgements

Vorrei innanzitutto ringraziare la mia famiglia per la possibilità datami nello svolgere questo percorso accademico e per avermi sempre incitato anche quando le cose non andavano nel migliore dei modi. Ringrazio mia morosa Nicole che in tutto questo percorso mi è sempre stata vicina e mi ha supportato e sopportato sempre. Voglio ringraziare i miei due fratelli acquisiti Baro e Conve con il quale ho passato bellissimi momenti fin dal primo giorno di università e che mi sono stati vicini nonostante in magistrale le nostre strade si siano divise, grazie ragazzi perchè senza di voi non sarei mai riuscito a raggiungere un così ottimo risultato. Ringrazio anche tutti gli altri compagni che nel bene o nel male hanno condiviso con me il percorso accademico e che mi hanno sempre aiutato in qualsiasi compito o che anche solo mi hanno dato una parola di conforto. Voglio ringraziare tutti gli amici con cui ho passato del tempo in questi anni e che mi hanno permesso di svagare e rimanere spensierato. Infine voglio ringraziare il prof.Tonin e soprattutto il dott.Tortora per avermi assegnato questo bellissimo progetto e per la pazienza avuta con me durante questo percorso.